J. Fluid Mech. (2012), *vol.* 690, *pp.* 16–50. © Cambridge University Press 2011
doi:10.1017/jfm.2011.364

Multilayer shallow water equations with complete Coriolis force. Part 2. Linear plane waves

Andrew L. Stewart and Paul J. Dellar†

OCIAM, Mathematical Institute, 24–29 St Giles', Oxford OX1 3LB, UK

(Received 18 December 2009; revised 26 June 2011; accepted 30 August 2011; first published online 25 November 2011)

We investigate the behaviour of linear plane waves in multilayer shallow water equations that include a complete treatment of the Coriolis force. These equations improve upon the conventional shallow water equations, based on the traditional approximation, that include only the part of the Coriolis force due to the locally vertical component of the rotation vector. Including the complete Coriolis force leads to dramatic changes in the structure of long linear plane waves. It allows subinertial waves to exist with frequencies below the inertial frequency, the minimum frequency for which waves exist under the traditional approximation. These subinertial waves are characterized by a distinguished limit in which the horizontal pressure gradient becomes comparable to the upwellings and downwellings driven by the non-traditional Coriolis term in the vertical momentum equation. The subinertial waves connect wave modes that remain separate in the conventional multilayer shallow water equations, such as the surface and internal waves in a two-layer system. Eastward-propagating surface waves in a two-layer system connect with westward-propagating internal waves, and vice versa, via the long subinertial waves. The long subinertial waves cannot be classified as either surface or internal waves, due to the phase difference between the disturbances to the interfaces in these waves.

Key words: ocean circulation, shallow water flows, waves in rotating fluids

1. Introduction

The large-scale dynamics of the Earth's oceans and atmosphere are dominated by the interaction of the Coriolis force and stratification, and involve complex phenomena over wide ranges of length and time scales. Simplifications and approximations are thus widely used in the attempt to formulate more tractable descriptions of different phenomena. In particular, it has become conventional to neglect the contribution to the Coriolis force associated with the locally horizontal component of the Earth's rotation vector. This approximation was named the 'traditional approximation' by Eckart (1960), and some of its consequences were reviewed by Gerkema *et al.* (2008). The 'non-traditional' terms in the Coriolis force may have a pronounced effect upon mesoscale flows such as Ekman spirals (Leibovich & Lele 1985) and deep convection (Marshall & Schott 1999), in lakes (Botte & Kay 2002), upon internal

† Email address for correspondence: dellar@maths.ox.ac.uk

https://doi.org/10.1017/jfm.2011.364 Published online by Cambridge University Press

waves (Gerkema & Shrira 2005*a*,*b*), and upon waves at near-inertial frequencies in weakly stratified regions of the ocean (van Haren & Millot 2005).

The traditional approximation may be formally derived as a small aspect ratio approximation, one that is valid when vertical length scales are small compared with horizontal length scales (e.g. White & Bromley 1995; White *et al.* 2005). Some of the recent interest in re-evaluating the traditional approximation is driven by the increasing resolutions of numerical simulations, which now reach horizontal length scales for which the traditional approximation becomes questionable. For example, in 1992 the UK Meteorological Office abandoned the traditional approximation in their unified model for the atmosphere (Cullen 1993). Similarly, the traditional approximation is sometimes justified as being valid in the dispersion relation for internal waves when the buoyancy or Brunt–Väisälä frequency N is much larger than the inertial frequency f (Phillips 1968, 1973; Hendershott 1981). However, the oceans contain substantial wave activity at or near inertial frequencies (Munk & Phillips 1968; Fu 1981), and regions of very weak stratification where the Brunt–Väisälä or buoyancy frequency N is less than 10 times the inertial frequency (Munk 1981). van Haren & Millot (2005) found areas of the Mediterranean with little or no stratification ($N = 0 \pm 0.4f$) to within the uncertainty of their measurements.

Shallow water equations are widely used as conceptual models in geophysical fluid dynamics. They also form the basis of many three-dimensional numerical models that use a Lagrangian discretization in the vertical, such as the Miami Isopycnal Coordinate Ocean Model (MICOM) described by Bleck *et al.* (1992) and Bleck & Chassignet (1994). Two-layer shallow water models are particularly widely used, because they capture some of the baroclinic effects that arise in continuously stratified fluids, such as internal waves (e.g. LeBlond & Mysak 1978) and baroclinic instability (e.g. Phillips 1954; Boss, Paldor & Thompson 1996; Vallis 2006). They describe the troposphere and the stratosphere (e.g. Vallis 2006), the upper mixed layer and the lower ocean (e.g. LeBlond & Mysak 1978; Salmon 1982), and deep ocean currents flowing beneath relatively quiescent fluid (e.g. Nof & Olson 1993). All of these models are conventionally derived using the traditional approximation. Dellar & Salmon (2005) showed that the complete Coriolis force could be included in shallow water equations for a single fluid layer flowing over a prescribed bottom topography. Stewart & Dellar (2010) extended this work to include arbitrarily many superposed layers. Dellar (2011) rederived the single-layer equations as an asymptotically consistent β-plane approximation for a small region of a spheroidal Earth.

In this paper we analyse linear plane waves in the non-traditional shallow water equations. The behaviour of such waves under the traditional approximation is well documented (e.g. Zeitlin 2007), as they provide a simple description of the behaviour of large-scale internal waves in the ocean. Hughes (1964), Saint-Guily (1970) and LeBlond & Mysak (1978) have given dispersion relations for internal waves in a continuously stratified fluid with the complete Coriolis force. These dispersion relations are anisotropic, because the horizontal component of the rotation vector defines a preferred horizontal direction. Moreover, waves may exist with frequencies below the inertial frequency $f = 2\Omega \sin\phi$, where ϕ is the latitude and Ω is the magnitude of the Earth's rotation vector. Such waves do not exist under the traditional approximation.

Thuburn, Wood & Staniforth (2002*a*,*b*) studied the effects of relaxing the traditional approximation on linear waves in a continuously stratified fluid on a sphere, and on the non-traditional analogue of the standard f-plane. They identified a scaling for long waves on an f-plane that is analogous to the scaling we find in § 3.3, and identified

https://doi.org/10.1017/jfm.2011.364 Published online by Cambridge University Press

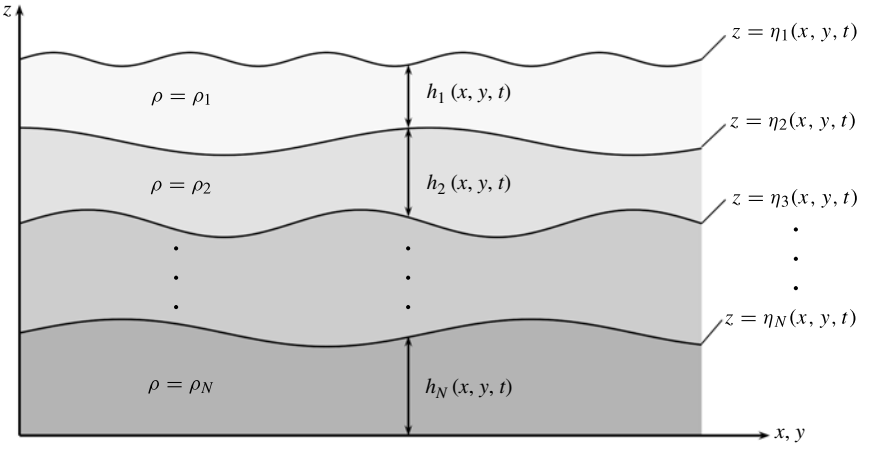


FIGURE 1. A schematic of the multilayer shallow water model.

new subinertial wave modes that do not exist under the traditional approximation. Kasahara (2003) began an extended, primarily numerical, study of linear waves in continuously stratified fluids on non-traditional analogues of f-planes and β-planes (Kasahara & Gary 2010). Kasahara (2007) studied non-traditional effects for linear initial value problems, in contrast to other work based on normal mode analyses. These studies identified a family of waves involving non-traditional effects that are characterized by large vertical wavenumbers, wavenumbers that tend to infinity in the limit of vanishing non-traditional effects. These waves are localized at horizontal boundaries. Gerkema & Exarchou (2008) surveyed the properties of non-traditional waves propagating through multiple weakly stratified fluid layers. They found that the non-traditional components of the Coriolis force permit near-inertial waves to be transmitted between layers of different stratifications, whereas the propagation of these waves may be blocked by a rapid change in the stratification under the traditional approximation.

Gerkema & Shrira (2005*a*,*b*) drew attention to the properties of the subinertial waves that arise in a continuously stratified fluids when the traditional approximation is not made. Our non-traditional multilayer shallow water equations also support a family of long subinertial waves, with a modal structure that differs from the usual surface and internal waves. In a multilayer system, the fast surface wave mode connects to the slowest internal wave mode through the long subinertial waves, while under the traditional approximation the different modes remain entirely separate. Long, energetic, internal waves in the ocean, those with wavelengths around 180 km according to § 6, are thus substantially affected by the complete Coriolis force. The range of wavenumbers for which the subinertial waves exist appears to increase to infinity in the limit of infinitely many layers, which would be consistent with the findings of Gerkema & Shrira (2005*b*) for the continuously stratified case.

2. The multilayer shallow water equations with complete Coriolis force

Stewart & Dellar (2010) derived equations to describe the behaviour of multiple superposed layers of inviscid, incompressible fluids with constant densities in a frame rotating about an arbitrary axis, as sketched in figure 1. The layers are labelled by $i = 1, \ldots, N$. Each layer has a dimensional density ρ_i, thickness $\tilde{h}_i(x, y, t)$,

https://doi.org/10.1017/jfm.2011.364 Published online by Cambridge University Press

pressure $\tilde{p}_i(x, y, z, t)$, horizontal velocity $\tilde{\boldsymbol{u}}_i = (\tilde{u}_i(x, y, z, t), \tilde{v}_i(x, y, z, t))$ and vertical velocity $\tilde{w}_i(x, y, z, t)$. We non-dimensionalize the three-dimensional Euler equations within each layer using

$$\boldsymbol{x} = \frac{\tilde{\boldsymbol{x}}}{R_d}, \quad z = \frac{\tilde{z}}{H}, \quad t = 2\Omega\tilde{t}, \quad \boldsymbol{u}_i = \frac{\tilde{\boldsymbol{u}}_i}{\sqrt{gH}}, \quad w_i = \frac{\tilde{w}_i}{2\Omega H}, \quad p_i = \frac{\tilde{p}_i}{\rho_i g H} \tag{2.1}$$

where the tilde ($\tilde{}$) denotes a dimensional variable. We have non-dimensionalized heights using a typical layer depth H and horizontal lengths using the Rossby deformation radius $R_d = \sqrt{gH}/(2\Omega)$ defined using the full Ω rather than its local vertical component Ω_z. The governing equations in the ith layer are

$$\frac{\partial \boldsymbol{u}_i}{\partial t} + (\boldsymbol{u}_i \cdot \boldsymbol{\nabla})\,\boldsymbol{u}_i + w_i \frac{\partial \boldsymbol{u}_i}{\partial z} + \Omega_z \hat{\boldsymbol{z}} \times \boldsymbol{u}_i + \varepsilon \boldsymbol{\Omega} \times \hat{\boldsymbol{z}} w_i + \boldsymbol{\nabla} p_i = 0, \tag{2.2a}$$

$$\varepsilon^2 \left(\frac{\partial w_i}{\partial t} + \boldsymbol{u}_i \cdot \boldsymbol{\nabla} w_i + w_i \frac{\partial w_i}{\partial z} \right) + \varepsilon(\Omega_x v_i - \Omega_y u_i) + \frac{\partial p_i}{\partial z} + 1 = 0, \tag{2.2b}$$

$$\boldsymbol{\nabla} \cdot \boldsymbol{u}_i + \frac{\partial w_i}{\partial z} = 0. \tag{2.2c}$$

Shallow water theory is based on the smallness of the ratio of vertical to horizontal length scales,

$$\varepsilon = \frac{H}{R_d} = 2\Omega\sqrt{\frac{H}{g}} \ll 1. \tag{2.3}$$

The non-traditional Coriolis terms are proportional to ε, while the vertical acceleration is proportional to ε^2. For typical parameters, $g = 9.8$ m s^{-1}, $\Omega = 7.3 \times 10^{-5}$ rad s^{-1} and $H = 500$ m, the ratio of length scales is small, $\varepsilon \approx 10^{-3}$. However, as our subsequent analysis of linear plane waves shows, the importance of non-traditional effects in internal motions is more accurately represented by replacing g in (2.3) with a reduced gravity $g' = g\Delta\rho/\rho$, where ρ is a typical density and $\Delta\rho$ is a typical density difference between adjacent layers. This internal aspect ratio, based on an internal deformation radius for the horizontal length scale, may be as large as $\varepsilon_{internal} \approx 0.1$, since $\Delta\rho/\rho$ may be as small as 10^{-4} in parts of the ocean.

Equations (2.2*a*)–(2.2*c*) are formulated in a pseudo-Cartesian coordinate system with the z-axis pointing radially outwards, antiparallel to the local gravitational acceleration. Such coordinates are commonly used to represent the behaviour in some limited region of the Earth's surface (e.g. Gill 1982; Pedlosky 1987; Salmon 1998; White 2002; Vallis 2006). They are *pseudo*-Cartesian because the horizontal x and y coordinate lines lie within a curved surface of constant geopotential, even though the resulting curvature terms in the metric are neglected (Phillips 1973; Dellar 2011). We have written the dimensionless horizontal and vertical components of the Earth's rotation vector as $\boldsymbol{\Omega} = (\Omega_x, \Omega_y)$ and Ω_z, respectively. It is convenient to rotate axes so that waves propagate parallel to the x-axis. We thus write

$$\Omega_x = \cos\phi \sin\theta, \quad \Omega_y = \cos\phi \cos\theta, \quad \Omega_z = \sin\phi, \tag{2.4}$$

where θ is the angle between the x-axis and the eastward direction, and ϕ is the latitude. The conventional axes in geophysical fluid dynamics correspond to taking $\theta = 0$. In principle, ϕ should vary with $\boldsymbol{x}$, but in the present work we take ϕ to be constant, thus restricting our attention to waves whose wavelengths are short compared

https://doi.org/10.1017/jfm.2011.364 Published online by Cambridge University Press

with the Earth's radius. This approximation was named the non-traditional f-plane by Gerkema & Shrira (2005*a*).

The different layers, each described by (2.2*a*)–(2.2*c*), are coupled by boundary conditions on the pressure and vertical velocity at the interfaces between layers. Stewart & Dellar (2010) discussed these boundary conditions in detail. The pressure at the free surface of the uppermost layer must be equal to the atmospheric pressure,

$$p_1 = P_{atm} = \frac{\tilde{P}_{atm}}{\rho_1 g H} \quad \text{at } z = \eta_1, \tag{2.5}$$

where $\tilde{P}_{atm}$ is the dimensional atmospheric pressure (assumed constant). The dimensional pressure must also be continuous at all internal surfaces. In dimensionless variables this becomes

$$\rho_i p_i = \rho_{i-1} p_{i-1} \quad \text{on } z = \eta_i, \quad \text{for } i = 2, \ldots, N. \tag{2.6}$$

Particles on each internal surface must remain on that surface, so $(\mathrm{D}/\mathrm{D}t)(z - \eta_i) = 0$ at $z = \eta_i$ for $i = 2, \ldots, N$. This must hold in the fluid on each side of the surface $z = \eta_i$, so we obtain a pair of kinematic boundary conditions at each surface,

$$\frac{\partial \eta_i}{\partial t} + \boldsymbol{u}_{i-1} \cdot \boldsymbol{\nabla} \eta_i = w_{i-1}, \quad \frac{\partial \eta_i}{\partial t} + \boldsymbol{u}_i \cdot \boldsymbol{\nabla} \eta_i = w_i \quad \text{on } z = \eta_i, \quad \text{for } i = 2, \ldots, N. \tag{2.7}$$

This may be interpreted as imposing continuity of the normal velocity at the surface $z = \eta_i$. Finally, we require the velocity normal to the bottom boundary to be zero, so $w_N = 0$ on $z = 0$.

Stewart & Dellar (2010) derived the multilayer shallow water equations from (2.2*a*)–(2.2*c*) by expanding the governing equations asymptotically in ε and averaging in z across each layer, and also by averaging the action in Hamilton's principle. We present a shorter, although somewhat less rigorous, derivation by assuming from the outset that the fluid moves strictly in columns, $\boldsymbol{u} = \boldsymbol{u}(x, y, t)$ with no z-dependence. We treat the aspect ratio $\varepsilon \ll 1$ as a small parameter, and neglect the $O(\varepsilon^2)$ vertical acceleration in (2.2*b*). This approximation was named the quasihydrostatic approximation by White & Bromley (1995). It extends the hydrostatic approximation by retaining the non-traditional Coriolis terms in the vertical momentum equation, but still omits the vertical acceleration. We may then integrate (2.2*b*) and (2.2*c*) with respect to z to obtain expressions for the pressure and vertical velocity in each layer,

$$p_i = p_i|_{z=\eta_i} + (\eta_i - z)(1 + \varepsilon(\Omega_x v_i - \Omega_y u_i)), \tag{2.8}$$

$$w_i = w_i|_{z=\eta_{i+1}} + (\eta_{i+1} - z)\boldsymbol{\nabla} \cdot \boldsymbol{u}_i. \tag{2.9}$$

The pressure in each layer acquires a contribution from every layer above it, and the vertical velocity in each layer is affected by the movement of all internal surfaces below it. We calculate these contributions by applying (2.6) and (2.7) repeatedly to (2.8) and (2.9),

$$p_i = (\eta_i - z)(1 + \varepsilon(\Omega_x v_i - \Omega_y u_i)) + \sum_{j=1}^{i-1} \frac{\rho_j}{\rho_i} h_j (1 + \varepsilon(\Omega_x v_j - \Omega_y u_j)), \tag{2.10}$$

$$w_i = \boldsymbol{\nabla} \cdot (\eta_{i+1} \boldsymbol{u}_i) - z \boldsymbol{\nabla} \cdot \boldsymbol{u}_i - \sum_{j=i+1}^{N} \boldsymbol{\nabla} \cdot (h_j \boldsymbol{u}_j). \tag{2.11}$$

We complete the derivation by substituting (2.10) and (2.11) into the horizontal momentum equation (2.2*a*), and integrating from $z = \eta_{i+1}$ to $z = \eta_i$ in the ith layer.

https://doi.org/10.1017/jfm.2011.364 Published online by Cambridge University Press

A rigorous treatment requires a z-dependent $O(\varepsilon)$ correction to the velocity, $\boldsymbol{u} = \boldsymbol{u}^{(0)}(x, y, t) + \varepsilon \boldsymbol{u}^{(1)}(x, y, z, t)$, in order to balance the z-dependent $O(\varepsilon)$ terms in w_i and $\boldsymbol{\nabla} p_i$. Stewart & Dellar (2010) discuss this in detail, and obtain the same shallow water momentum equation (2.13) as a consistent approximation that is accurate to order ε. A key step is the result $\overline{u\,v} = \overline{u}\,\overline{v} + O(\varepsilon^2)$ if $u = \overline{u} + O(\varepsilon)$ and $v = \overline{v} + O(\varepsilon)$ are both nearly independent of z, and $\overline{u}$ denotes the depth average of a quantity u.

Following Wu (1981), we derive the shallow water mass conservation equation for the ith layer

$$\frac{\partial h_i}{\partial t} + \boldsymbol{\nabla} \cdot (h_i \overline{\boldsymbol{u}}_i) = 0, \tag{2.12}$$

in terms of the depth-averaged velocity $\overline{\boldsymbol{u}}_i$, by integrating the incompressibility condition (2.2*c*) from $z = \eta_{i+1}$ to $z = \eta_i$. Finally, we integrate (2.2*a*) over each layer and rearrange using (2.12) to obtain the shallow water momentum equation with complete Coriolis force,

$$\begin{aligned}\frac{\partial \overline{\boldsymbol{u}}_i}{\partial t} + (\overline{\boldsymbol{u}}_i \cdot \boldsymbol{\nabla})\overline{\boldsymbol{u}}_i + \left(\Omega_z - \frac{1}{2}\varepsilon\, \boldsymbol{\Omega} \cdot \boldsymbol{\nabla}(\eta_i + \eta_{i+1})\right) \hat{\boldsymbol{z}} \times \overline{\boldsymbol{u}}_i + \frac{1}{2}\varepsilon\, \boldsymbol{\Omega} \times \hat{\boldsymbol{z}} \frac{\partial}{\partial t}(\eta_i + \eta_{i+1}) \\ + \boldsymbol{\nabla} \left\{ \eta_i + \frac{1}{2}\varepsilon h_i (\overline{v}_i \Omega_x - \overline{u}_i \Omega_y) + \frac{1}{\rho_i} \sum_{j=1}^{i-1} \rho_j h_j (1 + \varepsilon(\overline{v}_j \Omega_x - \overline{u}_j \Omega_y)) \right\} = 0. \end{aligned} \tag{2.13}$$

The Coriolis acceleration due to the vertical velocity w_i in the (2.2*a*) corresponds approximately to the non-traditional term proportional to $\partial_t(\eta_i + \eta_{i+1})$ in (2.13), whilst the quasihydrostatic pressure (2.8) leads to the appearance of non-traditional terms in the pressure gradient. The final non-traditional term corrects the traditional planetary vorticity Ω_z. The complete planetary vorticity in the ith layer, $\Omega_z - (1/2)\varepsilon\, \boldsymbol{\Omega} \cdot \boldsymbol{\nabla}(\eta_i + \eta_{i+1})$, is the component of the Earth's rotation vector normal to the layer's midsurface (Stewart & Dellar 2010). This expression may also be interpreted as the layer average of an Ertel potential vorticity formulated using Lagrangian labels in the vertical (Dellar & Salmon 2005). In the following we drop the overbar notation on $\overline{\boldsymbol{u}}_i$.

3. Linear plane waves in the two-layer shallow water equations

In this section we analyse the behaviour of linear plane waves in the non-traditional two-layer shallow water equations. This illustrates the effect of including the complete Coriolis force on both barotropic and baroclinic waves in the simplest possible setting. The two-layer case also serves as a useful point of reference for our analysis of linear plane waves in three or more layers in § 4. The non-traditional two-layer shallow water equations may be obtained by setting $i = 1, 2$ and $\eta_3 = 0$ in (2.12) and (2.13),

$$\begin{aligned}\frac{\partial \boldsymbol{u}_1}{\partial t} + (\boldsymbol{u}_1 \cdot \boldsymbol{\nabla})\boldsymbol{u}_1 + \left[\Omega_z - \varepsilon\, \boldsymbol{\Omega} \cdot \boldsymbol{\nabla}\left(h_2 + \frac{1}{2}h_1\right)\right] \hat{\boldsymbol{z}} \times \boldsymbol{u}_1 \\ + \boldsymbol{\nabla}\left[h_2 + h_1 + \frac{1}{2}\varepsilon\, h_1 (v_1 \Omega_x - u_1 \Omega_y)\right] \\ - \varepsilon\, \boldsymbol{\Omega} \times \hat{\boldsymbol{z}} \boldsymbol{\nabla} \cdot \left(\frac{1}{2}h_1 \boldsymbol{u}_1 + h_2 \boldsymbol{u}_2\right) = 0, \end{aligned} \tag{3.1a}$$

$$\frac{\partial h_1}{\partial t} + \boldsymbol{\nabla} \cdot (h_1 \boldsymbol{u}_1) = 0, \tag{3.1b}$$

https://doi.org/10.1017/jfm.2011.364 Published online by Cambridge University Press

$$\frac{\partial \boldsymbol{u}_2}{\partial t} + (\boldsymbol{u}_2 \cdot \boldsymbol{\nabla})\boldsymbol{u}_2 + \left[\Omega_z - \frac{1}{2}\varepsilon\, \boldsymbol{\Omega} \cdot \boldsymbol{\nabla} h_2\right] \hat{\boldsymbol{z}} \times \boldsymbol{u}_2 - \varepsilon\, \boldsymbol{\Omega} \times \hat{\boldsymbol{z}} \boldsymbol{\nabla} \cdot \left(\frac{1}{2} h_2 \boldsymbol{u}_2\right)$$
$$+ \boldsymbol{\nabla}\left[h_2 + \rho_r h_1 + \frac{1}{2}\varepsilon\, h_2(v_2\Omega_x - u_2\Omega_y) + \rho_r \varepsilon\, h_1(v_1\Omega_x - u_1\Omega_y)\right] = 0, \quad (3.1c)$$

$$\frac{\partial h_2}{\partial t} + \boldsymbol{\nabla} \cdot (h_2 \boldsymbol{u}_2) = 0. \quad (3.1d)$$

where $\rho_r = \rho_1/\rho_2$ is the density ratio. In constructing (3.1*a*) and (3.1*c*), we have used the mass conservation equations (3.1*b*) and (3.1*d*) to remove the time derivatives of h_1 and h_2 from (2.13).

The behaviour of linear plane waves in the traditional two-layer shallow water equations is well established in geophysical fluid dynamics (e.g. Gill 1982, § 6.2), as they offer an intuitive description of the interaction of rotation and stratification in large-scale wave phenomena. When rotating uniformly about a vertical axis, the equations are invariant to rotations of the horizontal axes, and so the behaviour of linear waves is isotropic. The only inter-dependence between layers is through the pressure gradient, as may be seen in (3.1*a*) and (3.1*c*) by setting $\varepsilon = 0$. This simple vertical structure allows the linearized equations to be exactly decomposed into barotropic and baroclinic modes (e.g. Zeitlin 2007), corresponding to surface waves and internal waves, respectively.

When the complete Coriolis force is included, (3.1*a*) and (3.1*c*) are no longer invariant under rotations about the vertical axis, so the behaviour of linear waves should be anisotropic. Dellar & Salmon (2005) showed that this is the case for linear waves in the non-traditional single-layer shallow water equations. In the non-traditional two-layer equations we also expect to see a disruption of the vertical structure, because vertically aligned fluid columns in different layers lie at different distances from the oblique axis of rotation. In this section we show that the waves modes make a transition from barotropic to baroclinic modes at long wavelengths, so the modes can no longer be decomposed. In the range of wavelengths over which this transition takes place, the structure of the waves changes dramatically, and they are no longer recognizable as either surface waves or internal waves.

3.1. *Dispersion relation*

We consider an equilibrium state in which the dimensional heights of both layers are constant, $\tilde{h}_1 = H_1$ and $\tilde{h}_2 = H_2$, and the fluid velocities are zero, $\boldsymbol{u}_1 = \boldsymbol{u}_2 = 0$. We choose $H = H_1$ as the height scale for our non-dimensionalization in (2.1), so the dimensionless equilibrium heights are $h_1 = 1$ and $h_2 = R$, where $R = H_2/H_1$ is the ratio of layer thicknesses. It is straightforward to show that this steady state is a solution of the two-layer equations (3.1*a–d*). We perturb the equilibrium state by setting $\boldsymbol{u}_1 = \boldsymbol{u}_1'$, $h_1 = 1 + h_1'$, $\boldsymbol{u}_2 = \boldsymbol{u}_2'$, and $h_2 = R + h_2'$, where $|\boldsymbol{u}_1'|, |h_1'|, |\boldsymbol{u}_2'|, |h_2'| \ll 1$. Substituting into (3.1*a–d*) and neglecting products of small terms, we obtain

$$\frac{\partial \boldsymbol{u}_1'}{\partial t} + \Omega_z \hat{\boldsymbol{z}} \times \boldsymbol{u}_1' - \varepsilon\, \boldsymbol{\Omega} \times \hat{\boldsymbol{z}} \boldsymbol{\nabla} \cdot \left(\frac{1}{2}\boldsymbol{u}_1' + R\boldsymbol{u}_2'\right)$$
$$+ \boldsymbol{\nabla}\left[(h_1' + h_2') + \frac{1}{2}\varepsilon(v_1'\Omega_x - u_1'\Omega_y)\right] = 0, \quad (3.2a)$$

$$\frac{\partial h_1'}{\partial t} + \boldsymbol{\nabla} \cdot \boldsymbol{u}_1' = 0, \quad (3.2b)$$

https://doi.org/10.1017/jfm.2011.364 Published online by Cambridge University Press

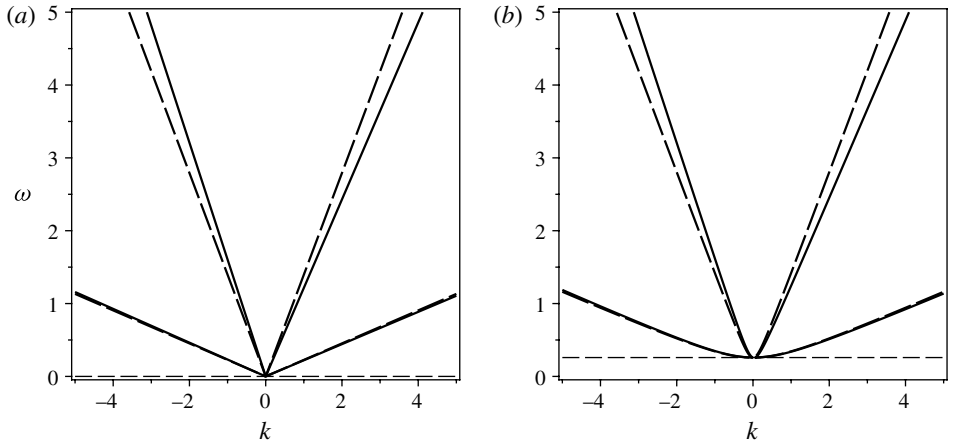


FIGURE 2. Dispersion curves for traditional (thick dashed lines) and non-traditional (solid lines) east/west-propagating waves at (*a*) the equator and (*b*) at 15° N (right), with parameters $\varepsilon = 0.2$, $\sigma = 0.1$ and $R = 1$. The horizontal thin dashed line marks the inertial frequency.

$$\frac{\partial \boldsymbol{u}_2'}{\partial t} + \Omega_z \hat{\boldsymbol{z}} \times \boldsymbol{u}_2' - \frac{1}{2}\varepsilon R\, \boldsymbol{\Omega} \times \hat{\boldsymbol{z}} \nabla \cdot \boldsymbol{u}_2' + \nabla(h_2' + \rho_r h_1') + \nabla\left[\frac{1}{2}\varepsilon R(v_2'\Omega_x - u_2'\Omega_y) + \rho_r \varepsilon (v_1'\Omega_x - u_1'\Omega_y)\right] = 0, \tag{3.2c}$$

$$\frac{\partial h_2'}{\partial t} + R\nabla \cdot \boldsymbol{u}_2' = 0. \tag{3.2d}$$

We seek plane wave solutions of the form $\boldsymbol{u}_1', h_1', \boldsymbol{u}_2', h_2' \sim \exp[\mathrm{i}(kx + ly - \omega t)]$. The wave vector $\boldsymbol{k} = (k, l)$ defines the direction of propagation in the horizontal plane. For convenience we choose θ, the orientation of the x- and y-axes, such that the x-axis points in the direction of the wave vector. Our perturbations are therefore proportional to $\exp[\mathrm{i}(kx - \omega t)]$, and θ defines the direction of wave propagation. Note that θ appears in (3.2*a–d*) only through the horizontal component of the rotation vector $\boldsymbol{\Omega}$, so we expect the behaviour of waves to be anisotropic only when the complete Coriolis force is included. Substituting $\boldsymbol{u}_1', h_1', \boldsymbol{u}_2', h_2' \sim \exp[\mathrm{i}(kx - \omega t)]$ into (3.2*a–d*) yields a matrix of coefficients whose determinant must be zero to guarantee non-trivial solutions for the perturbation velocities and layer thicknesses,

$$\begin{aligned}
&\omega^4 + \varepsilon\, \Omega_y k(1 + R)\, \omega^3 \\
&\quad + \{-2\Omega_z^2 - k^2(1 + R) + \varepsilon^2 \Omega_y^2 \sigma R k^2 - \tfrac{1}{4}(1 + R^2 + 4R(1 - \sigma))\varepsilon^2 \Omega_x^2 k^2\}\omega^2 \\
&\quad + \{-\varepsilon\, \Omega_y \Omega_z^2 (1 + R)k - 2\,\sigma\varepsilon\, \Omega_y R k^3 - \tfrac{1}{4}\varepsilon^3 \Omega_y \Omega_x^2 R(R + 1)k^3\}\omega \\
&\quad + \{\Omega_z^4 + k^4 \sigma R + \Omega_z^2\, k^2 R + \tfrac{1}{16} k^4 \varepsilon^4 \Omega_x^4 R^2 \\
&\quad + \tfrac{1}{4} k^2 \varepsilon^2 \Omega_x^2 (k^2 R(1 + R) + \Omega_z^2 (1 + R^2))\} = 0.
\end{aligned} \tag{3.3}$$

Here $\sigma = 1 - \rho_r = (\rho_2 - \rho_1)/\rho_2$ is the dimensionless density difference. There are also two geostrophic modes with $\omega = 0$, but they are not substantially altered by the non-traditional components of the Coriolis force.

Figure 2 shows some numerically generated plots of the dispersion relation (3.3), computed using relatively large values of σ and ε so that all of the dispersion curves are visible on the same plot. We show in § 3.5 that the waves with higher

https://doi.org/10.1017/jfm.2011.364 Published online by Cambridge University Press

frequency, and consequently larger phase velocities, are surface waves in which the free and internal surfaces move in phase. The lower-frequency waves are internal waves, in which the free surface is approximately flat and the internal surface oscillates. When the complete Coriolis force is included, the waves acquire an east/west asymmetry due to the θ-dependence of Ω_x and Ω_y. However, there is no substantial difference between the traditional and non-traditional frequencies for $O(1)$ wavelengths, i.e. dimensional wavelengths comparable to the deformation radius R_d. In the following we show that more dramatic changes occur for very short and very long waves.

3.2. *Asymptotic solutions*

There are formulae for the exact roots of a quartic polynomial such as (3.3) (e.g. Abramowitz & Stegun 1965), but such an approach is impractical for a quartic whose coefficients are already long algebraic expressions. Computed solutions, such as those shown in figure 2, are of limited use in describing the general behaviour of the waves, so instead we employ an asymptotic expansion in the small aspect ratio ε,

$$\omega = \omega_\varepsilon^{(0)} + \varepsilon\,\omega_\varepsilon^{(1)} + \varepsilon^2\omega_\varepsilon^{(2)} + \cdots. \tag{3.4}$$

Substituting into (3.3) and equating powers of ε gives the first three terms in this expansion,

$$\omega_\varepsilon^{(0)} = \pm_\alpha \sqrt{\sin^2\phi + \tfrac{1}{2}k^2\left(1 + R \pm_\beta \sqrt{(1+R)^2 - 4\sigma R}\right)}, \tag{3.5a}$$

$$\omega_\varepsilon^{(1)} = -\tfrac{1}{4}k\cos\phi\cos\theta\left(1 + R \pm_\beta \sqrt{(1+R)^2 - 4\sigma R}\right), \tag{3.5b}$$

$$\begin{aligned}\omega_\varepsilon^{(2)} = \frac{1}{16\omega_\varepsilon^{(0)}\sqrt{1+2R+R^2-4\sigma R}}\Bigg[&\pm_\beta 2R(1-\sigma)\sin^2(2\phi)\sin^2\theta \\ &\pm_\beta k^2\cos^2\phi\left\{(R+1)((R+1)^2 - 2R\sigma)\right. \\ &\left. + (R^2+1+2(1-\sigma)R(1+\sin^2\theta))\sqrt{(1+R)^2-4\sigma R}\right\}\Bigg].\end{aligned} \tag{3.5c}$$

The $\pm_\alpha$ and $\pm_\beta$ may take signs independently of one another, so the leading-order term $\omega_\varepsilon^{(0)}$ has four solutions as expected. These solutions are the wave frequencies under the traditional approximation. The higher-order terms $\omega_\varepsilon^{(1)}$ and $\omega_\varepsilon^{(2)}$ represent corrections due to non-traditional effects. These corrections depend on θ, so the non-traditional waves are indeed anisotropic. The linear dependence of $\omega_\varepsilon^{(1)}$ on k introduces the east/west asymmetry, decreasing the frequencies of eastward-propagating waves and increasing the frequencies of westward-propagating waves. However, $\omega_\varepsilon^{(1)} \to 0$ as $\theta \to \pm\pi/2$, and $\omega_\varepsilon^{(0)}$ and $\omega_\varepsilon^{(2)}$ are even functions of k, so we expect this asymmetry to vanish for northward- and southward-propagating waves. This is consistent with the governing equations (3.1*a–d*). The non-traditional components of the Coriolis force act longitudinally and vertically, but not latitudinally.

Setting $k = 0$ in the full dispersion polynomial (3.3) gives $\omega = \pm_\alpha \sin\phi$ regardless of the value of ε, so the frequency of very long waves must approach the inertial frequency as $k \to 0$. Setting $k = 0$ in our asymptotic expansion (3.5*a–c*) yields $\omega_\varepsilon^{(0)} = \pm_\alpha \sin\phi$, so the leading order term is exact and higher-order terms introduce

https://doi.org/10.1017/jfm.2011.364 Published online by Cambridge University Press

errors. The next term in the expansion is

$$\omega_\varepsilon^{(3)} \sim \pm_\beta \frac{R\sin^2\phi\cos^3\phi\,\cos\theta\sin^2\theta(1-\sigma)}{k\sqrt{(1+R)^2-4\sigma R}} = O\left(\frac{1}{k}\right) \quad \text{as } k \to 0, \tag{3.6}$$

so the expansion becomes disordered in the limit as $k \to 0$, and cannot describe the behaviour of long waves.

A natural alternative approach is to fix ε and pose an expansion of ω in powers of k instead,

$$\omega = \omega_k^{(0)} + k\omega_k^{(1)} + k^2\omega_k^{(2)} + \cdots. \tag{3.7}$$

This is guaranteed to remain ordered in the limit $k \to 0$, but is only valid for $k \ll 1$. Substituting (3.7) into the dispersion polynomial (3.3) and equating powers of k yields

$$\omega_k^{(0)} = \pm_\gamma \sin\phi, \tag{3.8a}$$

$$\omega_k^{(1)} = \tfrac{1}{4}\varepsilon\,\cos\phi\left[-(1+R)\cos\theta \pm_\delta \sqrt{(1-R)^2\cos^2\theta + 4R(1-\sigma)}\right], \tag{3.8b}$$

$$\omega_k^{(2)} = \pm_\gamma \frac{1}{16\sin\phi}\left\{4(1+R) + \varepsilon^2\cos^2\phi\left((1+R)^2 - 2\sigma R\right)\right.$$
$$\left. \mp_\delta \frac{\cos\theta\left((1+R)^2-4\sigma R\right)\left(4+\varepsilon^2(1+R)\cos^2\phi\right)}{\sqrt{\cos^2\theta\,(1-R)^2+4R(1-\sigma)}}\right\}. \tag{3.8c}$$

Here again we use subscripts $\pm_\gamma$ and $\pm_\delta$ to denote that these operators may take signs independently of one another. Note that $\omega_k^{(1)}$ is $O(\varepsilon)$, just as previously $\omega_\varepsilon^{(1)}$ was $O(k)$, so the two approximations $\omega_k^{(0)} + k\omega_k^{(1)}$ and $\omega_\varepsilon^{(0)} + \varepsilon\omega_\varepsilon^{(1)}$ coincide when k, ε and θ are all close to 0. However, the higher-order terms $\omega_k^{(n)}$ for $n \geqslant 3$ diverge as $\varepsilon \to 0$. We return to this in § 3.3.

The expansion (3.8*a–c*) shows that $\partial\omega/\partial k \neq 0$ at $k = 0$ when non-traditional effects are included ($\varepsilon \neq 0$). This means that some wave frequencies close to $k = 0$ must lie below the inertial frequency. Gerkema & Shrira (2005*b*) obtained an analogous result for linear waves in a continuously stratified fluid, and showed that the behaviour of very long waves ($k \to 0$) is independent of the stratification. Very long waves in the two-layer shallow water equations do depend on σ, the relative density difference between the layers, but they are only strongly affected when propagating almost eastward/westward. Restricting our attention to positive frequencies, the dispersion relation in the limit $k \to 0$ is

$$\omega = \sin\phi + \frac{\varepsilon\,k}{4}\cos\phi\left[-(1+R)\cos\theta \pm_\delta \sqrt{(1-R)^2\cos^2\theta + 4R(1-\sigma)}\right] + O(k^2). \tag{3.9}$$

Equation (3.9) is most easily interpreted by restricting $\theta \in [-\pi/2, \pi/2]$ so that $\cos\theta \geqslant 0$. Then $k > 0$ corresponds to eastward-propagating waves, and $k < 0$ corresponds to westward-propagating waves. The root corresponding to the negative branch of $\pm_\delta$ is always larger than the inertial frequency for $k < 0$, and always smaller for $k > 0$, so there is always one eastward-propagating subinertial wave mode. The root corresponding to the positive branch of (3.9) is smaller than the inertial frequency for $k > 0$ when $|\theta|$ is below the critical angle

$$\theta_c = \sin^{-1}\sqrt{\sigma}. \tag{3.10}$$

https://doi.org/10.1017/jfm.2011.364 Published online by Cambridge University Press

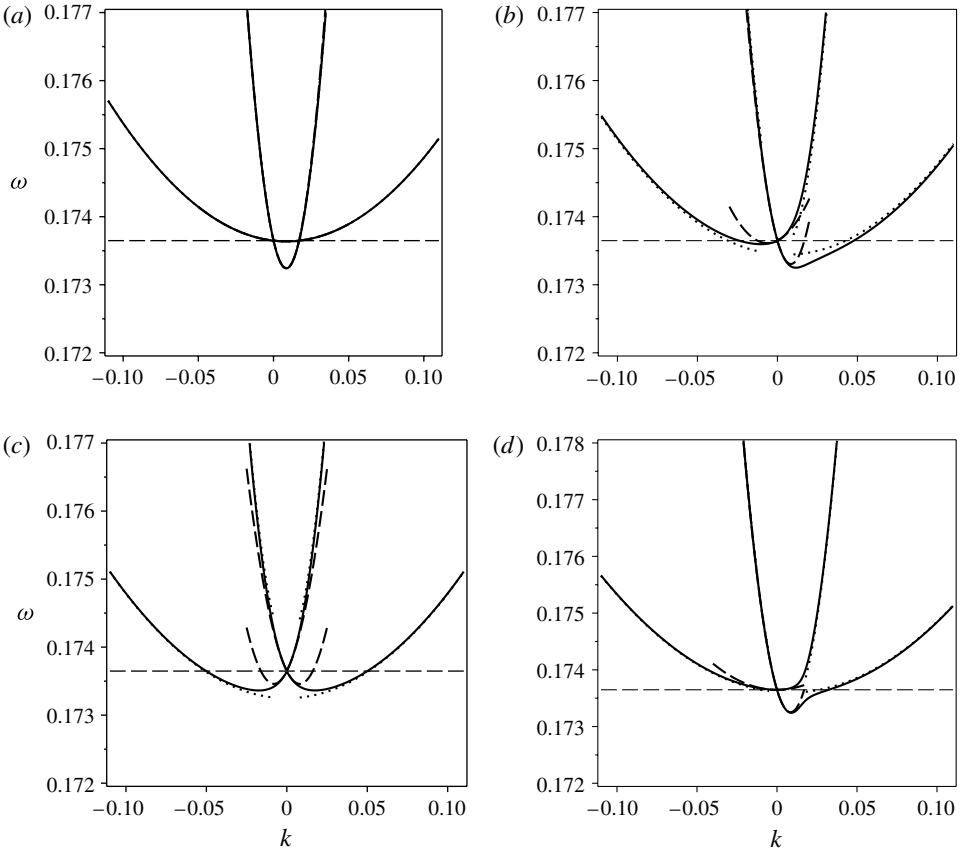


FIGURE 3. Long-wave dispersion curves for waves propagating (*a*) east/west, (*b*) northeast/southwest, (*c*) north/south and (*d*) at the critical angle. All plots are at 10° N with $\sigma = \varepsilon = 0.1$ and $R = 1$. Numerical solutions are shown solid, small ε asymptotic solutions using thick dashed lines, and small k asymptotic solutions using dotted lines. The horizontal thin dashed line marks the inertial frequency.

The second subinertial mode also propagates eastward if $|\theta| < \theta_c$, while if $|\theta| > \theta_c$ the second subinertial mode propagates westward. When $|\theta| = \theta_c$ there is only a single subinertial mode. As σ is typically very small ($\lesssim 10^{-3}$) in the ocean, we only expect to find two subinertial waves propagating in the same direction when $|\theta| \lesssim 2°$.

Figure 3 shows the long-wave dispersion relation for waves propagating in various directions. We have again used exaggerated values of σ and ε to make both the surface and internal wave branches visible on the same plot. Figure 3(*a*) shows the case of east/west-propagating waves, where the asymptotic solutions are indistinguishable from the numerical results. As predicted, the non-traditional terms lower the frequencies of eastward-propagating waves, and increase the frequencies in westward-propagating waves. Subinertial frequencies are present for both surface and internal waves, although the latter are difficult to see on these axes.

In fact, east/west-propagating waves ($\theta = 0$) are special cases, and the dispersion relation for northeast/southwest-propagating waves ($\theta = \pi/4$) shown in figure 3(*b*) is more typical. Here subinertial waves propagate in both directions because $\theta > \theta_c$. More importantly, one branch of the dispersion relation appears to correspond to a surface

https://doi.org/10.1017/jfm.2011.364 Published online by Cambridge University Press

wave mode for $k < 0$, but to an internal wave mode for $k > 0$. Similarly, the other branch corresponds to an internal wave mode for $k < 0$, and to a surface wave mode for $k > 0$. This transition is explored in § 3.5.

Figure 3(*d*) shows waves propagating at the critical angle θ_c, and confirms that there is only one subinertial wave. The shape of the non-traditional dispersion relation gives some insight into the transition from separate internal and surface wave branches when $\theta = 0$, to branches that change from surface to internal waves and vice versa when $\theta \neq 0$. For north/south-propagating waves, shown in figure 3(*c*), the dispersion curves are symmetric about $k = 0$, as predicted by our expansion for small ε, and the subinertial region encompasses the largest range of wavenumbers. This suggests that north/south-propagating long internal waves may be most influenced by non-traditional effects.

3.3. *A distinguished limit as* $\varepsilon, k \to 0$

Our small-k expansion was motivated by the breakdown of our small-ε expansion in the limit $k \to 0$. However, we encounter an equivalent breakdown of our small k expansion when ε is small. The leading-order term $\omega_k^{(0)}$ is accurate for any ε at $k = 0$, but the higher-order terms in k introduce an error. Similarly to (3.6) above, we find that

$$\omega_k^{(3)} \sim \pm_\delta \frac{R\sin^2\theta(1-\sigma)\left((1+R)^2 - 4\sigma R\right)}{2\,\varepsilon\cos\phi\sin^2\phi\left\{(1-R)^2\cos^2\theta + 4R(1-\sigma)\right\}^{3/2}} = O\left(\frac{1}{\varepsilon}\right) \quad \text{as } \varepsilon \to 0, \tag{3.11}$$

so the expansion in k becomes disordered when $\varepsilon = O(k)$. This mutual disordering suggests a combined asymptotic limit as both $k, \varepsilon \to 0$. We seek a scaling

$$k = \varepsilon^a K, \tag{3.12}$$

with some exponent a, such that we obtain the global behaviour of the solution from letting $\varepsilon \to 0$ while K remains $O(1)$. We determine a by requiring that both our existing asymptotic expansions remain bounded as $\varepsilon, k \to 0$. That is, we require that $\varepsilon^i \omega_\varepsilon^{(i)} \to 0$ and $k^i \omega_k^{(i)} \to 0$ as $\varepsilon, k \to 0$ for all i. For latitude $\phi \neq 0$ and $i \geqslant 1$, it may be shown that $\omega_\varepsilon^{(i)} \sim k^{2-i}$ as $k \to 0$, and similarly that $\omega_k^{(i)} \sim \varepsilon^{2-i}$ as $\varepsilon \to 0$. Using the scaling (3.12), we therefore require that

$$\left.\begin{aligned} \varepsilon^i \omega_\varepsilon^{(i)} &\sim \varepsilon^i k^{(2-i)} = \varepsilon^{i+a(2-i)} K^{2-i} \\ k^i \omega_k^{(i)} &\sim k^i \varepsilon^{2-i} = \varepsilon^{ai+(2-i)} K^i \end{aligned}\right\} \to 0 \quad \text{as } \varepsilon \to 0,\ i \geqslant 1. \tag{3.13}$$

We therefore require $i + a(2-i) > 0$ and $ai + (2-i) > 0$ for all $i \geqslant 1$. This immediately yields $a > 0$ from the cases $i = 1$ and $i = 2$, and for $i \geqslant 3$ rearranges into the constraints

$$1 - \frac{2}{i} < a < \left(1 - \frac{2}{i}\right)^{-1} \quad \text{for } i \geqslant 3. \tag{3.14}$$

whose only solution is $a = 1$. Hence, $k = \varepsilon K$ is the appropriate scaling to study the distinguished limit as $\varepsilon, k \to 0$.

A more physical motivation for the scaling $k = \varepsilon K$ may be obtained directly from the linearized equations (3.2). For plane waves proportional to $\exp[\mathrm{i}(kx - \omega t)]$ the two continuity equations (3.2*b*) and (3.2*d*) become

$$\omega h_1' = k u_1', \quad \omega h_2' = R k u_2'. \tag{3.15}$$

https://doi.org/10.1017/jfm.2011.364 Published online by Cambridge University Press

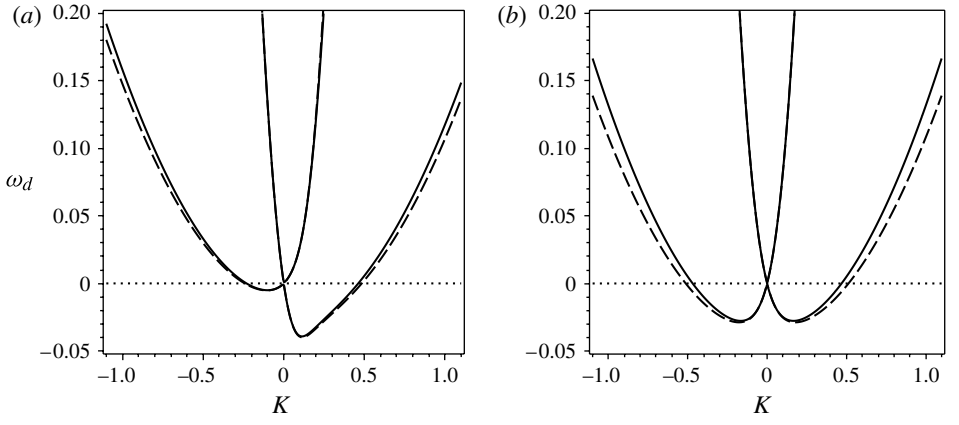


FIGURE 4. Dispersion relations for waves propagating (*a*) northeast/southwest and (*b*) north/south, at 10° N with $\varepsilon = 0.2$. Here $K = k/\varepsilon$ is the rescaled wavenumber, and $\omega_d = (\omega - \sin\phi)/\varepsilon^2$ is the rescaled deviation of the frequency from the inertial frequency. Numerical solutions are shown as solid curves and the asymptotic solutions in the distinguished limit are shown as dashed curves.

The frequency ω remains $O(1)$ as $k \to 0$, at any latitude $\phi \neq 0$, so we must have $h_1', h_2' \to 0$ as $k \to 0$. At $k = 0$, the linearized shallow water momentum equations (3.2*a*) and (3.2*c*) reduce to

$$\omega \boldsymbol{u}_1' + \mathrm{i}\Omega_z \hat{\boldsymbol{z}} \times \boldsymbol{u}_1' = 0, \quad \omega \boldsymbol{u}_2' + \mathrm{i}\Omega_z \hat{\boldsymbol{z}} \times \boldsymbol{u}_2' = 0. \tag{3.16}$$

Their solution describes inertial oscillations in each layer with frequency $\pm\omega = \Omega_z$, the vertical component of the dimensionless planetary vorticity. The velocity perturbations u_1' and u_2' thus remain $O(1)$ as $k \to 0$. From (3.15), we deduce that the height perturbations h_1' and h_2' are proportional to k as $k \to 0$. In other words, for long waves the perturbations to the free and internal surfaces become vanishingly small relative to the velocity perturbations. We now evaluate the relative magnitudes of terms in the x component (3.2*a*) of the momentum equation,

$$\omega u_1' - \mathrm{i}\Omega_{z0} v_1' + \varepsilon \Omega_y k(\tfrac{1}{2}u_1' + R u_2') - k(h_1' + h_2' + \tfrac{1}{2}\varepsilon(v_1'\Omega_x - u_1'\Omega_y)) = 0. \tag{3.17}$$

The pressure gradient $k(h_1' + h_2')$ is $O(k^2)$, while the non-traditional terms are $O(\varepsilon k)$, as $k \to 0$. The non-traditional terms thus become comparable in magnitude to the hydrostatic pressure gradient for sufficiently long waves with $k = O(\varepsilon)$.

Setting $k = \varepsilon K$, the dispersion relation (3.3) contains only even powers of ε. This motivates an asymptotic expansion of the form

$$\omega = \omega^{(0)} + \varepsilon^2 \omega^{(1)} + \varepsilon^4 \omega^{(2)} + \cdots. \tag{3.18}$$

Collecting terms in powers of ε^2, the $O(1)$ solution is

$$\omega^{(0)} = \pm \sin\phi. \tag{3.19}$$

At $O(\varepsilon^2)$, we obtain a quadratic polynomial that determines $\omega^{(1)}$,

$$\sin^2\phi\,\omega^{(1)2} + \tfrac{1}{2}K \sin\phi(\cos\theta\cos\phi\sin\phi \mp K)\omega^{(1)} + \tfrac{1}{4}K^2 R(K\sigma(K \mp 2\cos\phi\sin\phi\cos\theta) - \cos^2\phi\sin^2\phi(\sin^2\theta - \sigma)) = 0. \tag{3.20}$$

https://doi.org/10.1017/jfm.2011.364 Published online by Cambridge University Press

These roots describe four wave modes, depending on which sign of the $\mp$ operator is taken. Figure 4 shows the wave frequencies when $k = O(\varepsilon)$. Following the above scalings, we plot the deviation of the solution from the inertial frequency, $\omega_d = (\omega - \sin\phi)/\varepsilon^2$, against the scaled wavenumber $K = k/\varepsilon$, which gives a universal picture of the dispersion relation as $\varepsilon \to 0$ with $k = O(\varepsilon)$. The leading-order approximation to ω_d is $\omega^{(1)}$. We use a very large value $\varepsilon = 0.2$ to make the distinction between the asymptotic and numerical solutions visible in figure 4.

3.4. *Properties of subinertial waves*

The combination of (3.19) and (3.20) accurately captures the behaviour of long waves, and allows us to derive some analytical results for long subinertial waves. We first obtain an estimate for the wavelength at which non-traditional effects become important by determining the width of the subinertial region, i.e. the non-zero wavenumbers at which the frequency is again equal to the inertial frequency. Setting $\omega^{(1)} = 0$ and solving for K yields

$$k_{inert} = \tfrac{1}{2}\varepsilon \sin(2\phi)(\cos\theta \pm \sin\theta\sqrt{1/\sigma - 1}), \tag{3.21}$$

which confirms that the width of the subinertial range of wavenumbers is $O(\varepsilon)$ as $\varepsilon \to 0$. For $|\theta| \leqslant \pi/2$ we may rearrange (3.21) to show that both solutions for k_{inert} are only positive when $|\theta| < \theta_c$, as defined in (3.10). We thus recover our earlier result from § 3.2 for the direction of propagation of subinertial waves.

A straightforward conversion back to dimensional variables gives a dimensional wavenumber $\tilde{k} \sim H/R_d^2$ that is much larger than any oceanographic length scale. However, the width is also $O(\sigma^{-1/2})$ when the density ratio σ is small. Subinertial waves become much shorter in weakly stratified layers, and in § 4 we will show that this scaling changes to $k_{inert} \sim \varepsilon/\sigma$ for three or more layers.

The approximate solution (3.21) is not valid in the limit $\sigma \to 0$ for fixed ε. We may obtain an exact expression for k_{inert} by setting $\omega = \sin\phi$ in the dispersion relation (3.3) and solving for k. In this case k_{inert} depends on the layer depth ratio R, whereas the approximate expression (3.21) does not, so we set $R = 1$ for simplicity. The exact expression is

$$k_{inert} = \frac{\varepsilon\,\Omega_z\left(\sigma\Omega_y + \frac{1}{4}\varepsilon^2\Omega_y\Omega_x^2 \pm \Omega_x\sqrt{(1-\sigma)\left(\sigma + \frac{1}{2}\varepsilon^2\Omega_x^2 + \frac{1}{16}\varepsilon^4\Omega_x^2(\Omega_y^2 + \Omega_x^2)\right)}\right)}{\sigma + \frac{1}{2}\varepsilon^2\Omega_x^2 + \frac{1}{16}\varepsilon^4\Omega_x^4} \tag{3.22}$$

where Ω_x, Ω_y and Ω_z are the dimensionless components of the rotation vector, as defined in (2.4). There are $O(\varepsilon^2)$ terms in the denominator of (3.22), so (3.21) is only valid for σ finite.

Equation (3.21) implies that the subinertial region will be widest when $\theta = \pm\pi/2$, corresponding to north/south-propagating waves. Hughes (1964) showed that poleward-propagating waves in a continuously stratified fluid could not travel beyond a critical latitude ϕ_c, which was expressed by Gerkema *et al.* (2008) as

$$\phi_c = \pm\sin^{-1}\left[\frac{\tilde{\omega}^2}{4\Omega^2} - \frac{\tilde{\omega}^2}{N^2}\left(\frac{\tilde{\omega}^2}{4\Omega^2} - 1\right)\right]^{1/2}, \tag{3.23}$$

where $\tilde{\omega}$ is the dimensional wave frequency and N is the buoyancy or Brunt–Väisälä frequency.

These analyses use ray theory (e.g. Whitham 1974; LeBlond & Mysak 1978) to study the behaviour of waves on a sphere using the dispersion relation for waves on

https://doi.org/10.1017/jfm.2011.364 Published online by Cambridge University Press

an f-plane. The ray theory approximation is valid for wavelengths much smaller than the radius of the Earth, and allows the latitude ϕ to be treated as a parameter in the f-plane dispersion relation $\tilde{\omega} = \tilde{\omega}(\mathbf{k}; \phi)$. According to ray theory, a wavepacket propagates poleward with constant frequency $\tilde{\omega}_0$ equal to its initial frequency, and a changing wave vector $\mathbf{k}$ determined by the dispersion relation $\tilde{\omega}(\mathbf{k}; \phi) = \tilde{\omega}_0$. The critical latitude ϕ_c is the value of ϕ for which waves with frequency $\tilde{\omega}_0$ cease to exist in the f-plane dispersion relation. Making the traditional approximation is equivalent to taking $N \to \infty$ in (3.23), so the critical latitude becomes equal to the inertial latitude, the latitude at which the inertial frequency $2\Omega \sin\phi$ equals the wave frequency $\tilde{\omega}$ (Gerkema *et al.* 2008). Non-traditional effects allow waves to exist with frequencies below the inertial frequency.

To obtain a similar result for our two-layer system we use (3.20) to find the minimum frequency ω_{min}. This arises when $k = k_{min}$, given by

$$k_{min} = \pm\frac{1}{2}\varepsilon \sin(2\phi) \left(\frac{(1-\sigma)\sqrt{R}}{(1+R+2\sqrt{\sigma R})\sqrt{\sigma}} \right)^{1/2} + O\left(\varepsilon^3\right). \tag{3.24}$$

Using (3.19) and (3.20), we rewrite the minimum frequency as

$$\omega_{min} = |\sin\phi| \left(1 - \frac{1}{2}\varepsilon^2 \cos^2\phi \frac{(1-\sigma)R}{1+R+2\sqrt{\sigma R}} + O\left(\varepsilon^4\right) \right). \tag{3.25}$$

Poleward-propagating waves of a given frequency ω only exist at latitudes for which $\omega_{min} < \omega$. The so-called turning latitude ϕ_c, at which incident waves must be reflected, is given by $\omega = \omega_{min}$, so (3.25) gives

$$\sin\phi_c = \pm\omega \left(1 + \frac{1}{2}\varepsilon^2 (1-\omega^2) \frac{(1-\sigma)R}{1+R+2\sqrt{\sigma R}} \right) + O\left(\varepsilon^4\right). \tag{3.26}$$

Including the complete Coriolis force shifts the turning latitude poleward by an $O(\varepsilon^2)$ distance. There is an analogy between this result and the turning latitude for the waves in a continuously stratified Boussinesq fluid, as studied by Gerkema & Shrira (2005*a*,*b*). For strong stratification with $N \gg 2\Omega$ the minimum frequency is (Gerkema *et al.* 2008)

$$\omega_{min} = |\sin\phi| \left(1 - \tfrac{1}{2}\kappa^2 \cos^2\phi + O(\kappa^4)\right), \tag{3.27}$$

where $\kappa = 2\Omega/N \ll 1$. This may be rearranged to give an expression for the turning latitude,

$$\sin\phi_c = \pm\omega \left(1 + \tfrac{1}{2}\kappa^2 (1-\omega^2)\right) + O(\kappa^4). \tag{3.28}$$

In this case, including the complete Coriolis force shifts the turning latitude poleward by an $O(\kappa^2)$ distance. Gerkema & Shrira (2005*a*) showed that this poleward shift persists when the latitudinal variation of Ω_z is included under the β-plane approximation. However, in a vertically bounded domain, incident waves may become trapped at the turning latitude at the bottom of the ocean. If the stratification varies with depth, $N = N(z)$, then so does the latitude at which waves are reflected. There is then no longer a clearly defined turning latitude for the waves.

The similarity between the forms of (3.28) and (3.26) suggests that the role of κ in the continuously-stratified case is similar to that of ε in our layered model. As $\varepsilon = H/R_d = 2\Omega\sqrt{H/g}$ and $\kappa = 2\Omega/N = 2\Omega/\sqrt{-g/\rho_0\,\mathrm{d}\rho/\mathrm{d}z}$, where ρ_0 is a reference density and $\rho(z)$ is the stratification, our layer height H is analogous to the density

https://doi.org/10.1017/jfm.2011.364 Published online by Cambridge University Press

scale height $-\rho_0/(\mathrm{d}\rho/\mathrm{d}z)$. The approximation (3.28) also follows from the more general expression (3.23) for the turning latitude by writing the dimensional frequency as $\tilde{\omega} = 2\Omega\omega$ and expanding the right-hand side of (3.23) in powers of κ. The quantity κ differs by a factor of $\sin\phi$ from the aspect ratio f/N that appears in the three-dimensional quasigeostrophic equations (e.g. Pedlosky 1987; White 2002). This factor is due to our use of Ω rather than $\Omega_z = \Omega\sin\phi$ in our definition of the deformation radius R_d. With this identification of ε in a layered model with κ in a continuously stratified fluid, our scaling for long near-inertial waves corresponds with the scaling for very shallow internal waves in Thuburn *et al.* (2002*b*).

Whilst the minimum frequency ω_{min} and the corresponding turning latitude ϕ_c have an interesting analogy with continuously stratified waves, the expansion (3.18) in the distinguished limit shows that the deviation of ω_{min} from the traditional case is only $O(\varepsilon^2)$. A more dynamically relevant property is that the group velocity $c_g = \mathrm{d}\omega/\mathrm{d}k$ vanishes at $\omega = \omega_{min}$, so a packet of waves with wavenumbers around k_{min} would be stationary. Equation (3.24) shows that $k_{min} \sim \varepsilon/\sigma^{1/4}$, so these waves are even longer than the estimate (3.21) suggests, but our findings in § 4 suggest that they may be somewhat shorter in the case of multiple layers. A further consequence of the shift in k_{min} is that the inertial oscillations at $k = 0$ have non-zero group velocity when the non-traditional effects are accounted for, but this is less relevant to realistic oceanic motions. Gerkema & Shrira (2005*b*) found similar results for long waves in the continuously stratified case. The group velocity was again non-zero at $k = 0$, but there was no zero of the group velocity close to $k = 0$. Instead, the frequency decreased monotonically towards a minimum ω_{min} as $k \to \infty$.

3.5. *Structure of subinertial waves*

In § 3.4 we showed that relaxing the traditional approximation leads to interesting and unexpected changes in the wave frequencies. We now show that the structure of the waves also changes dramatically in the subinertial region created by the complete Coriolis force. We illustrate this by considering the relationship between the perturbations h_1' and h_2' to the layer thicknesses. For perturbations of the form $\exp[\mathrm{i}(kx - \omega t)]$, the linearized equations (3.2*a–d*) may be rearranged to give

$$r_h = \frac{h_1'}{h_2'} = \frac{4k^2 + 4\varepsilon k\left(\mathrm{i}\,\Omega_x\Omega_z - \omega\Omega_y\right) + 2\varepsilon^2 k^2\Omega_x^2}{4\omega^2 - 4\Omega_z^2 - 4k^2 + 4\omega\varepsilon k\Omega_y - \varepsilon^2 k^2\Omega_x^2}. \tag{3.29}$$

The imaginary term in the numerator of r_h causes the layer heights to oscillate out of phase. This does not occur under the traditional approximation ($\varepsilon = 0$). We first consider the behaviour of r_h when k is not close to 0. Using our asymptotic expansion (3.4) for ω in powers of ε, we expand (3.29) as

$$r_h = \frac{2}{R - 1 \pm_\beta \sqrt{(1+R)^2 - 4\sigma R}}\left(1 + \mathrm{i}\,\varepsilon\,\frac{\sin\theta\,\sin(2\phi)}{2k} + O(\varepsilon^2)\right) \quad \text{as } \varepsilon \to 0, \tag{3.30}$$

where $\pm_\beta$ takes the same sign as in (3.5*a*). The leading-order term is equal to that obtained under the traditional approximation, and is independent of the wavenumber. The positive root is approximately equal to $1/R = H_1/H_2$, and corresponds to h_1' and h_2' oscillating together. This gives rise to surface waves. The negative root is approximately equal to -1, so $h_1' + h_2' \approx 0$. This root corresponds to internal waves. Including non-traditional terms leads to an $O(\varepsilon)$ complex correction to the eigenmode, which causes the surfaces to oscillate slightly out of phase. This effect will be least pronounced for very short waves ($k \to \infty$), and most pronounced in

https://doi.org/10.1017/jfm.2011.364 Published online by Cambridge University Press

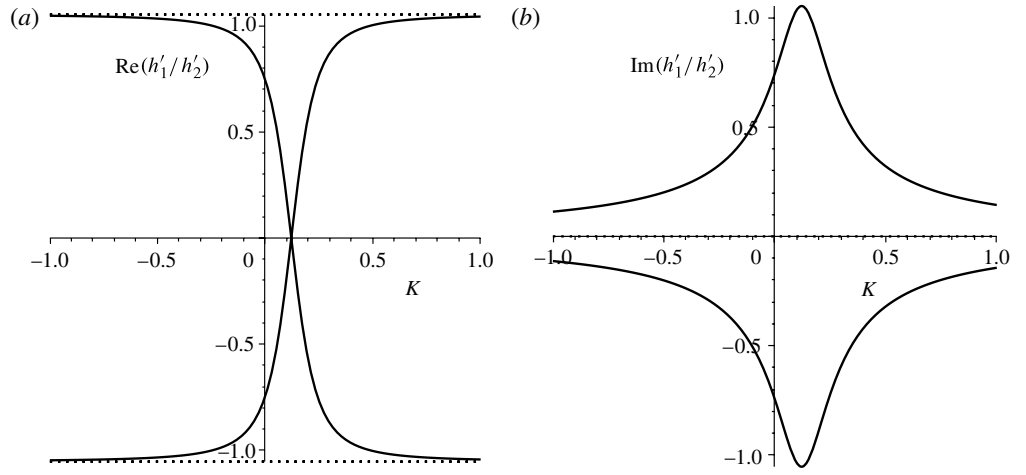


FIGURE 5. The (*a*) real and (*b*) imaginary parts of the perturbation height ratio $r_h = h_1'/h_2'$ for traditional (dotted lines) and non-traditional (solid lines) long waves propagating northeast/southwest at 10° N with $\sigma = \varepsilon = 0.1$ and $R = 1$.

long waves ($k \to 0$), although we cannot accurately consider the latter limit using an expansion in ε alone, as shown in § 3.3.

We obtain a similar expansion of r_h in powers of k by substituting (3.7) into (3.29). However, only the leading-order term is simple enough to interpret directly,

$$r_h = \frac{2(\pm_\gamma \mathrm{i}\,\sin\theta - \cos\theta)}{(1-R)\cos\theta \pm_\delta \sqrt{(1-R)^2\cos^2\theta + 4R(1-\sigma)}} + O(k) \quad \text{as } k \to 0, \tag{3.31}$$

where $\pm_\gamma$ and $\pm_\delta$ take the same signs as in (3.8*a*) and (3.8*b*). There is an $O(1)$ complex contribution to r_h at $k = 0$, even as $\varepsilon \to 0$, which identifies the traditional approximation as a singular limit. In other words, for ε arbitrarily close to zero, there is an $O(1)$ change in the wave structure for sufficiently small k.

To obtain a reliable picture of the behaviour of r_h close to $k = 0$, we use the distinguished limit expansion from § 3.3. We may use this to obtain an expansion of $r_h(K)$ in powers of ε, but we omit this result because it is difficult to interpret. Instead we present plots of the real and imaginary parts of r_h as functions of $K = k/\varepsilon$ in figure 5. We have used the same parameter values that we used to plot the dispersion curves for northeast/southwest-propagating waves in figure 4, and we show only the wave modes with positive frequencies. The real part of r_h makes a transition from surface to internal waves, or vice versa, in the range of subinertial wavenumbers. The complex part of r_h also becomes most prominent in the subinertial region, peaking when the real part reaches zero. The waves in the subinertial region are thus neither surface nor internal waves, so their structure has been dramatically altered by the inclusion of non-traditional terms. This alteration of the structure disappears at the equator ($\phi = 0$) and in east/west-propagating waves ($\theta = 0$), and is most prominent in north/south-propagating waves at midlatitudes.

In figure 6 we illustrate the alteration of the wave structure by the non-traditional components of the Coriolis force. We plot schematic profiles of the upper surface $z = \eta_1$ of a wave whose internal surface $z = \eta_2$ has a cosine profile, for $R = 1$ and $\sigma \ll 1$. Under the traditional approximation, the upper surface profiles distinctly correspond to a surface wave mode and an internal wave mode. In the non-traditional

https://doi.org/10.1017/jfm.2011.364 Published online by Cambridge University Press

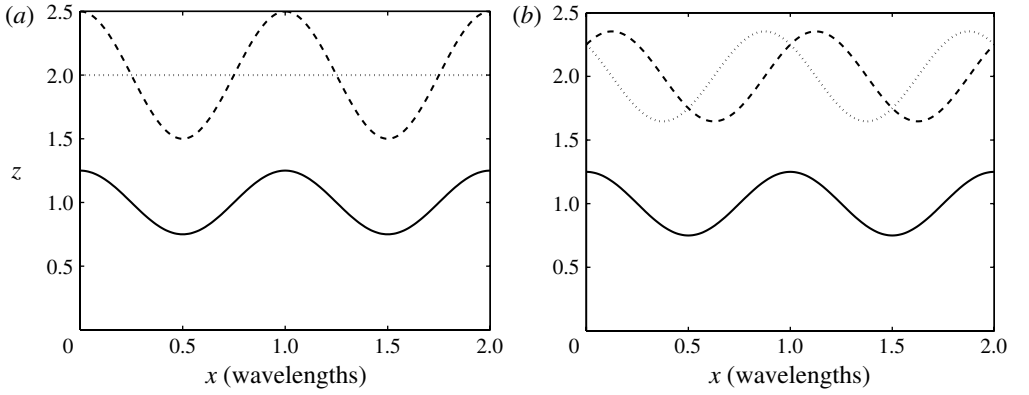


FIGURE 6. A schematic plot of the surface heights in linear plane waves close to the inertial frequency. Panel (*a*) shows the height of upper surface $z = \eta_1$ for both the surface (dashed line) and internal (dotted line) wave modes, for a fixed internal surface profile $z = \eta_2$. Panel (*b*) shows the same modes with non-traditional effects included, for the wavenumber in figure 5 at which $r_h = 0$.

case, corresponding to the wavenumber at which $r_h = 0$ in figure 5, the upper surface oscillates out of phase with the internal surface in both modes of propagation. This may constrain the amplitude of long internal waves, because perturbations to the internal surface require even larger perturbations to the upper surface when the complete Coriolis force is included. Under the traditional approximation the upper surface may remain approximately flat while the internal surface undulates. The principal restoring force acting on the internal surface is the reduced gravity, so perturbations to the internal surface require less energy than perturbations to the upper surface, which are subject to the full force of gravity. Thus, for the same wave energy, we expect long internal waves to have a smaller amplitude when the complete Coriolis force is included.

3.6. *Structure of short waves*

Non-traditional plane waves also exhibit some interesting structural changes at short wavelengths, where the ratio of the layer depth to the wavelength is smaller. However, these changes tend not to be as dramatic as those associated with subinertial waves. Manipulating (3.2*a–d*) with all variables proportional to $\exp[\mathrm{i}(kx - \omega t)]$ gives an expression for the ratio of the lower layer velocities,

$$r_v = \frac{v_2'}{u_2'} = \frac{-\mathrm{i}\Omega_z + \dfrac{1}{2}\varepsilon k R \Omega_x}{\omega}. \tag{3.32}$$

Under the traditional approximation ($\varepsilon = 0$), r_v is purely imaginary. For long waves $\omega \to \pm\Omega_z$ and $r_v \to \mp\mathrm{i}$, so the longitudinal and horizontal transverse velocities are of equal magnitude, but oscillate $\pi/2$ radians out of phase. In other words, long waves are circularly polarized. For short waves $|\omega| \to \infty$ and $r_v \to 0$, so the transverse velocity vanishes and the waves are unaffected by rotation. These short waves thus resemble sound waves, using the analogy between shallow water theory and adiabatic gas dynamics with adiabatic exponent $\gamma = 2$, although they still have vertical velocities if one interprets shallow water theory as being an approximation to motions under the full three-dimensional fluid equations.

https://doi.org/10.1017/jfm.2011.364 Published online by Cambridge University Press

Including non-traditional effects leads to an additional real term proportional to k in the numerator of (3.32). In the short wave limit ω is also proportional to k,

$$\omega \sim \pm_\alpha k \sqrt{\frac{1}{2}\left(1 + R \pm_\beta \sqrt{(1+R)^2 - 4\sigma R}\right)} + O(\varepsilon) \quad \text{as } |k| \to \infty, \tag{3.33}$$

so we expect r_v to tend to a real constant as $|k| \to \infty$. For surface waves, corresponding to the '$+_\beta$' root, we exploit the density difference σ as a second small parameter to write

$$r_v \to \pm\frac{1}{2}\varepsilon \cos\phi \sin\theta \, \frac{R}{\sqrt{1+R}} + O\left(\sigma\varepsilon, \varepsilon^2\right) \quad \text{as } |k| \to \infty, \tag{3.34}$$

while for internal waves, corresponding to the '$-_\beta$' root, we find

$$r_v \to \pm\frac{1}{2}\varepsilon \cos\phi \sin\theta \, \frac{R^{3/2}\sqrt{1+R}}{\sqrt{\sigma}} + O\left(\sigma^{1/2}\varepsilon, \sigma^{-1/2}\varepsilon^2\right) \quad \text{as } |k| \to \infty. \tag{3.35}$$

Non-traditional effects cause the transverse velocity to oscillate in phase with the longitudinal velocity, even in the short wave limit. The $\sqrt{\sigma}$ in the denominator of (3.35) makes the transverse velocity much more prominent in internal waves. The effective deformation radius of internal waves is smaller by a factor of $\sqrt{\sigma}$, since the restoring force due to buoyancy is weaker for internal waves. The effective aspect ratio between the vertical length scale and the relevant deformation radius is thus $\varepsilon/\sqrt{\sigma}$, as explained in § 5.

Equation (3.32) is analogous to the expression in Gerkema *et al.* (2008) for the ratio of the horizontal velocity perturbations in a continuously stratified fluid. In our notation, this expression becomes

$$\frac{|v'|}{|u'|} = \left|\frac{(\Omega_x \mu_\pm - \Omega_z)}{\omega}\right|, \quad \mu_\pm = \frac{\kappa^2 \Omega_x \Omega_z \pm \kappa\sqrt{\omega^2 - \Omega_z^2 + \kappa^2\omega^2(\Omega_x^2 - \omega^2 - \Omega_z^2)}}{1 + \kappa^2(\Omega_x^2 - \omega^2)} \tag{3.36}$$

Under the traditional approximation ($\Omega_x \equiv 0$) or close to the inertial frequency ($|\omega| \to |\Omega_z|$) we find that $v'/u' \to \pm\mathrm{i}$. Waves in a continuously stratified fluid thus become circularly polarized close to the inertial frequency, as in (3.32) for our two-layer system. If non-traditional effects are included, $\Omega_x = 0$ is only satisfied for east/west-propagating waves. For other directions of propagation, the term proportional to μ_+ in (3.36) causes the waves to become elliptically polarized close to the inertial frequency. van Haren & Millot (2004) discuss observations of such elliptically polarized near-inertial waves in weakly stratified regions of the Mediterranean Sea. A similar situation arises in the two-layer shallow water equations. The non-traditional part of (3.32) vanishes for infinitely long waves with $k = 0$ and $\omega = \Omega_z$, so these waves are circularly polarized. From (3.21), we know that there are one or two positive wavenumbers k_{inert} at which $\omega = \Omega_z$, and waves with these wavenumbers become elliptically polarized.

Figure 7 shows plots of the real and imaginary parts of r_v for waves with positive frequency. The corresponding plot for negative frequencies may be obtained by reflecting the left-hand plot about the vertical axis and the right-hand plot about the horizontal axis. The imaginary part of r_v is identical in the traditional and non-traditional cases, and represents the part of the transverse velocity that oscillates $\pi/2$ out of phase with the longitudinal velocity. This part is large for long waves, but

https://doi.org/10.1017/jfm.2011.364 Published online by Cambridge University Press

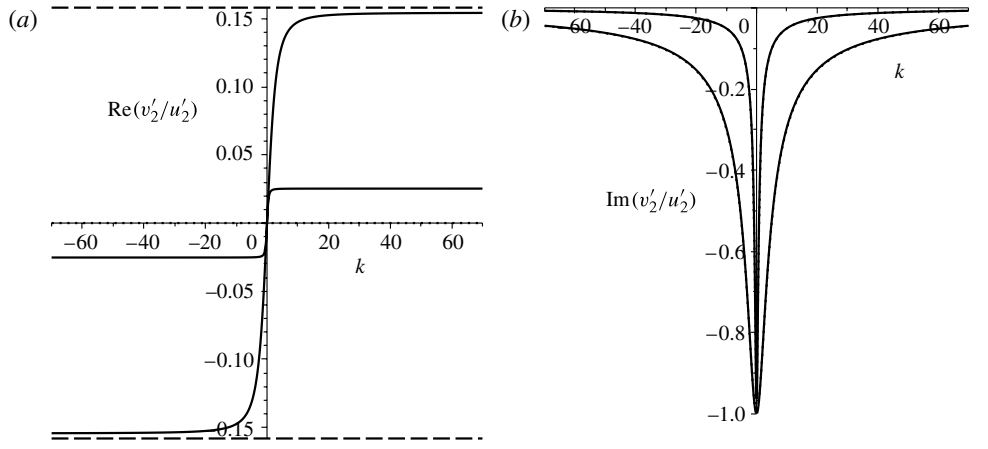


FIGURE 7. The (*a*) real and (*b*) imaginary parts of the ratio $r_v = v_2'/u_2'$ of the lower-layer perturbation velocities for traditional (dotted lines) and non-traditional (solid lines) long waves propagating northeast/southwest at 10° N with $\sigma = \varepsilon = 0.1$ and $R = 1$. The dashed line represents the asymptotic solution for infinitesimally short internal waves.

negligible for short waves, as described above. The plot also shows that the real part of the eigenmode only matches the traditional case ($r_v = 0$) at $k = 0$, while (3.35) gives the asymptotic behaviour of the real part of r_v as $|k| \to \infty$. The ratio v_1'/u_1' of the upper-layer velocities exhibits very similar behaviour to the behaviour we have shown for the ratio $r_v = v_2'/u_2'$ of lower-layer velocities.

Vertical velocities cause east/west accelerations in the three-dimensional Euler equations with the complete Coriolis force. Vertical motions appear in shallow water theory through changes in the layer depths, i.e. through $\partial_t h_1 = -\boldsymbol{\nabla} \cdot (h_1 \boldsymbol{u}_1)$ and $\partial_t h_2 = -\boldsymbol{\nabla} \cdot (h_2 \boldsymbol{u}_2)$, which is the origin of the divergence terms in (3.1*a*) and (3.1*c*). Oscillations of the layer heights therefore force oscillations of the transverse velocity for all but directly east/west-propagating waves. In the deep ocean, where the stratification is particularly small, the ratio of transverse to longitudinal velocities may be as large as 0.15 for internal waves.

4. Linear plane waves in the multilayer shallow water equations

In this section we extend our analysis of linear plane waves from § 3 to include three or more layers. Under the traditional approximation, increasing the number of layers leads to a predictable increase in the number of internal wave modes, so multilayer plane waves do not differ substantially from two-layer plane waves. However, as we have seen in § 3, including the complete Coriolis force connects the internal and surface modes at very long wavelengths, and it is not clear how these connections will change when more layers are added. We show here that two-layer plane waves are a special case whose frequency matches the inertial frequency when $k = k_{inert} \sim \varepsilon/\sqrt{\sigma}$. For multiple layers with equal relative density differences σ, this critical wavenumber is much larger, $k_{inert} \sim \varepsilon/\sigma$, so much shorter waves are influenced by the non-traditional components of the Coriolis force.

4.1. *Dispersion relation*

Each layer of fluid is governed by a set of shallow water equations, defined by (2.12) and (2.13). Following the approach detailed in § 3.1, linearizing the N-layer shallow

https://doi.org/10.1017/jfm.2011.364 Published online by Cambridge University Press

water equations yields a set of $3N$ equations for the $3N$ dependent variables u_i', v_i' and h_i'. Seeking solutions proportional to $\exp[\mathrm{i}(kx - \omega t)]$ and rearranging the equations, we obtain a polynomial of order $2N$ in ω, similar to (3.3),

$$\omega^{2N} + c_{2N-1}\omega^{2N-1} + \cdots + c_1\omega + c_0 = 0. \tag{4.1}$$

As in (3.3), we have factored out the N geostrophic modes with $\omega = 0$. Each coefficient c_n for $n = 1, \ldots, 2N-1$ is a function of k that depends on the layer thicknesses $R_i = H_i/H$, for $i = 1, \ldots, N$, the relative density differences $\sigma_i = (\rho_{i+1} - \rho_i)/\rho_{i+1}$, for $i = 1, \ldots, N-1$, the non-traditional parameter ε, the latitude ϕ and the direction of propagation θ. For $N > 2$ it is most efficient to proceed with the analysis using a symbolic manipulation package.

The solutions of (4.1) describe N wave modes of positive frequency ($\omega > 0$) and N wave modes of negative frequency ($\omega < 0$). We restrict our attention to the positive modes, because for every negative mode $\omega^{(-)}(k)$ there exists a positive mode $\omega^{(+)}(k)$ that satisfies $-\omega^{(+)}(k) = \omega^{(-)}(-k)$, and vice versa. Under the traditional approximation ($\varepsilon = 0$) the dispersion polynomial (4.1) contains no odd powers, $c_{2n-1} = 0$ for $n = 1, \ldots, N$, so it may be solved exactly for a larger number of layers. The dispersion relation in this case strongly resembles the traditional dispersion relation shown in figure 2, having one fast barotropic mode and $N-1$ slower baroclinic modes. The minimum frequency for all modes is the inertial frequency $\omega_{inert} = \sin\phi$.

Following our earlier analysis of the two-layer system we expect relaxing the traditional approximation (taking $\varepsilon \neq 0$) to produce little change in the dispersion relation at large wavenumbers. However, we expect non-traditional effects to be prominent close to $k = 0$. We may obtain the most complete picture of the behaviour close to $k = 0$ using the distinguished limit expansion described in § 3.3. For any number of layers, we set $k = \varepsilon K$ and substitute the expansion $\omega = \omega^{(0)} + \varepsilon^2\omega^{(1)} + \cdots$ into the dispersion polynomial (4.1). The leading-order solution for wave modes with positive frequencies is $\omega^{(0)} = \sin\phi$, as in (3.19). This satisfies the $O(\varepsilon^{2n})$ dispersion polynomial for $n = 0, \ldots, N-1$. At $O(\varepsilon^{2N})$ we obtain a polynomial of order N for the first correction $\omega^{(1)}$,

$$\omega^{(1)N} + \hat{c}_{N-1}\omega^{(1)N-1} + \cdots + \hat{c}_1\omega^{(1)} + \hat{c}_0 = 0. \tag{4.2}$$

The coefficients $\hat{c}_n$ are functions of K, σ_i, R_i, ϕ and θ, as in (4.1), but with no dependence on the non-traditional parameter ε.

In figure 8 we show the dispersion relation for typical parameters and increasing numbers of fluid layers. The deviation of the frequency from the inertial frequency in the slowest baroclinic mode becomes more pronounced for larger N. In the limit of infinitely many layers, we might expect to recover the continuously stratified results of Gerkema & Shrira (2005*b*), in which the frequency tends to a minimum as $k \to \infty$. We discuss this further in § 4.2. For any number of layers, the slowest baroclinic mode connects to the fast barotropic mode through the inertial frequency at $k = 0$. This may be shown by keeping ε fixed and considering the limit $k \to 0$, as in § 3.2. Substituting $\omega = \sin\phi + k\omega_k^{(1)} + \cdots$ into the dispersion polynomial (4.1) and collecting terms of $O(k^N)$, we obtain distinct non-zero solutions for the linear corrections $\omega_k^{(1)}$ to the inertial frequency. Each wave mode passes through the inertial frequency with a different group velocity, i.e. a different gradient in the k–ω plane. If the modes are only to cross at $k = 0$, the slowest mode must connect to the fastest, the second slowest to the second fastest, and so on. We have calculated the dispersion relations

https://doi.org/10.1017/jfm.2011.364 Published online by Cambridge University Press

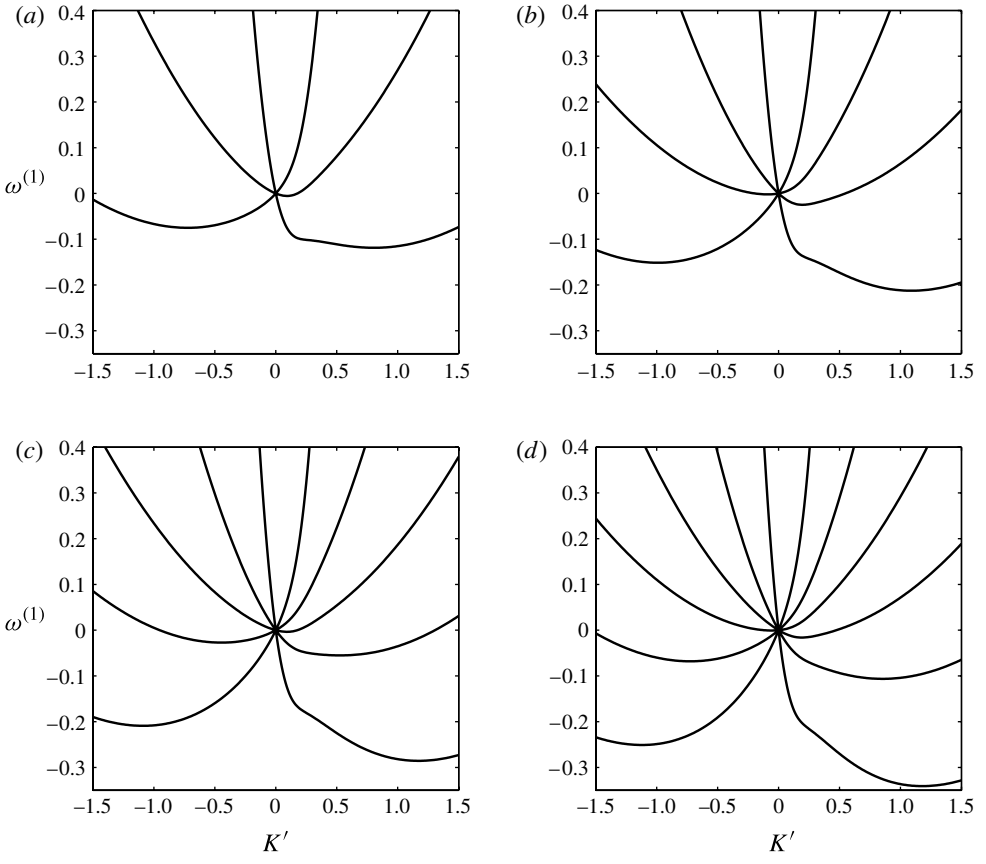


FIGURE 8. Dispersion relations for (*a*) three, (*b*) four, (*c*) five and (*d*) six layers of fluid of equal thickness, governed by the shallow water equations. The plots have been generated numerically using the distinguished limit $k = \varepsilon K$ with $K = O(1)$ as $\varepsilon \to 0$. Thus, $K = k/\varepsilon$ is the scaled dimensionless wavenumber, and $\omega^{(1)}$ is the $O(\varepsilon^2)$ correction to the inertial frequency $\omega^{(0)} = \sin\phi$. In each case $\phi = \pi/12$, $\theta = \pi/4$ and $\sigma_i = 0.1$ for $i = 1, \ldots, N-1$.

and verified these trends up to $N = 7$, as shown in figure 8, but for larger numbers of layers the algebra becomes prohibitively complicated.

4.2. *Inertial wavenumber*

As shown in § 3.4, including the complete Coriolis force dramatically alters the structure of waves in the range of subinertial wavenumbers. The wave modes exhibit $O(1)$ changes in the ratios of the layer depths at long wavelengths, and lose a clear distinction between surface waves and internal waves. A useful estimate of the wavelength at which the wave modes become strongly affected by the non-traditional components of the Coriolis force is k_{inert}, the wavenumber at which the wave frequency is equal to the inertial frequency. In two layers we showed that $k_{inert} \sim \varepsilon/\sqrt{\sigma}$ as $\varepsilon \to 0$ for fixed σ.

The complexity of the dispersion polynomial for N-layer plane waves (4.1) makes it difficult in general to obtain any analytical results about properties of subinertial waves. However, it is relatively straightforward to determine k_{inert} approximately using the distinguished limit with $k = O(\varepsilon)$ as $\varepsilon \to 0$. Substituting $\omega^{(1)} = 0$ into (4.2) yields a

https://doi.org/10.1017/jfm.2011.364 Published online by Cambridge University Press

polynomial in K,

$$\hat{c}_0(K) = \left(\prod_{i=1}^{N} R_i\right) K^N \left[\left(\prod_{i=1}^{N-1} \sigma_i\right) K^N + C_{N-1}K^{N-1} + \cdots + C_1 K + C_0\right] = 0. \quad (4.3)$$

The dimensionless layer depths R_i are all exact divisors of $\hat{c}_0(K)$, so the coefficients C_n depend only on ϕ, θ, and the density differences $\sigma_1, \ldots, \sigma_{N-1}$. The roots of (4.3) are the scaled inertial wavenumbers $K_{inert} = k_{inert}/\varepsilon$. Each wave mode passes through the inertial frequency twice, once at $k = 0$, which corresponds to one of the N roots $K = 0$ in (4.3), and again at a non-zero wavenumber that defines the inertial wavenumber for the mode.

Putting $N = 3$ into (4.3) gives the unscaled inertial wavenumbers for the three-layer shallow water equations,

$$k_{inert} = \frac{1}{2}\varepsilon \sin(2\phi)\cos\theta, \ \frac{1}{2}\varepsilon \sin(2\phi)\left(\cos\theta \pm \sin\theta\sqrt{\frac{1-\sigma_1\sigma_2}{\sigma_1\sigma_2}}\right). \quad (4.4)$$

The maximum inertial wavenumber scales as $k_{inert} \sim \varepsilon/\sqrt{\sigma_1\sigma_2}$, or as $k_{inert} \sim \varepsilon/\sigma$ if $\sigma_1 = \sigma_2 = \sigma$. The range of subinertial wavenumbers is thus considerably larger in three layers than it is in two, for which $k_{inert} \sim \varepsilon/\sqrt{\sigma}$. We find the same scaling for k_{inert} when more than three layers are included. For example, in five layers the largest roots for k_{inert} are

$$k_{inert} = \frac{1}{2}\varepsilon \sin(2\phi)\left(\cos\theta \pm_\alpha \frac{\sin\theta}{\sigma}\sqrt{\frac{1}{2}(1-\sigma)\left(3+\sigma \pm_\beta \sqrt{5-2\sigma+\sigma^2}\right)}\right), \quad (4.5)$$

where $\pm_\alpha$ and $\pm_\beta$ may take signs separately, and we have chosen $\sigma_1 = \sigma_2 = \sigma_3 = \sigma_4 = \sigma$ for simplicity. For $N > 5$ it is still possible to show that the largest inertial wavenumber satisfies $k_{inert} \sim \varepsilon/\sigma$, but the algebra involved in finding more detailed expressions becomes prohibitively complicated.

The exact formula for k_{inert} may be obtained for small N, and in certain special cases, by setting $\omega = \sin\phi$ in the dispersion polynomial (4.1) and solving for k. The exact general formula for $N = 2$ is given in (3.22). Our expressions (4.4) and (4.5) for k_{inert} are derived using the distinguished limit $k = O(\varepsilon)$ as $\varepsilon \to 0$, and by expanding ω in powers of ε^2. They are only accurate approximations to the exact formulae for k_{inert} when $\varepsilon^2 \ll \sigma$. We illustrate this in figure 9(*a*), where we plot the maximum inertial wavenumber k_{inert} against the density difference σ for $N = 4$. We fix $\varepsilon = 10^{-3}$, $R_1 = R_2 = R_3 = R_4 = 1$ and $\sigma_1 = \sigma_2 = \sigma_3 = \sigma$, so the system describes four layers with equilibrium depths of approximately 500 m, and with equal relative density differences. We use $\theta = \pi/2$ and $\phi = \pi/4$, corresponding to north/south-propagating waves at 45°N, because this allows us to obtain an exact expression for k_{inert}, and because (4.4) and (4.5) suggest that these parameters should maximize k_{inert}. The solution calculated using the distinguished limit begins to diverge substantially from the exact solution when $\sigma \approx \varepsilon^2 = 10^{-6}$.

In figure 9(*b*) we illustrate the change in the maximum inertial wavenumber k_{inert} as the number of layers increases. We have calculated the points marked by white circles by fixing $\theta = \pi/2$, $\phi = \pi/4$, $\varepsilon = 10^{-3}$, $R_i = 1$ for $i = 1, \ldots, N$ and $\sigma_i = 10^{-4}$ for $i = 1, \ldots, N-1$, so that we isolate changes in k_{inert} due to changes in N alone. Incrementing N by 1 corresponds to stacking an additional 500 m thick layer of fluid on top of the existing layers, whose density is 0.01 % less than the density of the layer

https://doi.org/10.1017/jfm.2011.364 Published online by Cambridge University Press

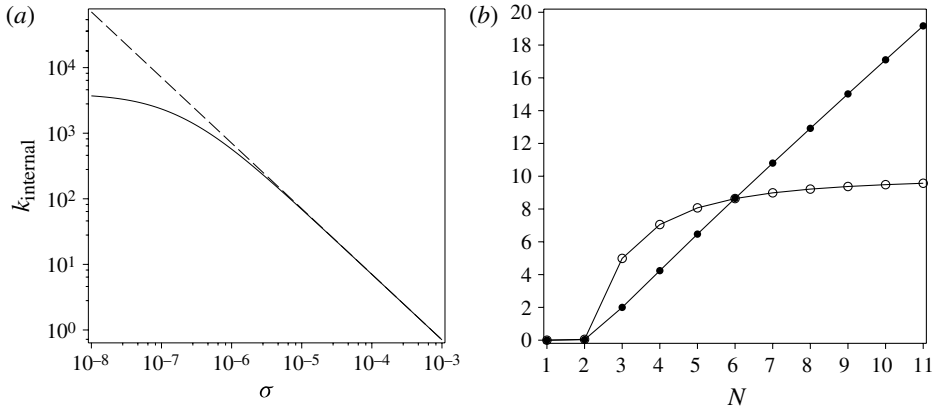


FIGURE 9. Plots of the maximum inertial wavenumber k_{inert} against (*a*) the density difference between layers, σ, and (*b*) the number of layers, N. In each case the waves propagate north/south ($\theta = \pi/2$) at 45°N ($\phi = \pi/4$), and the relative density differences are all equal, $\sigma_i = \sigma$, $R_i = R$. In (*a*), $N = 4$, $R = 1$, $\varepsilon = 10^{-3}$, and we vary σ. In (*b*), the white circles correspond to $R = 1$, $\sigma = 10^{-4}$, $\varepsilon = 10^{-3}$, and we vary N alone. The black circles correspond to a layer of fixed depth, $\varepsilon = 2 \times 10^{-3}$, $R = 1/N$ and fixed total density difference, $\sigma = 10^{-3}/(N-1)$.

immediately below. The maximum inertial wavenumber increases with N, but it grows so slowly for larger N that it may approach a limiting value as $N \to \infty$. This limit is somewhat artificial, as 11 layers corresponds to a total depth of 5500 m, which is close to the maximum depth of any ocean on Earth.

The points marked by black circles in figure 9(*b*) correspond to a more physically relevant case, in which we choose a fixed total equilibrium depth of $H = 2000$ m as our vertical length scale. This defines $\varepsilon \approx 2 \times 10^{-3}$ from (2.3), and also defines the horizontal length scale as $R_d \approx 960$ km. For a given number of layers N, we divide the total layer depth equally between the layers, so $R_i = 1/N$ for $i = 1, \ldots, N$. We also keep the total absolute density difference between the first and last layers approximately constant by setting $\sigma_i^{(N)} = \sigma_1^{(2)}/(N-1)$ for $i = 1, \ldots, N-1$, where $\sigma_i^{(N)}$ is the relative density difference between layers i and $i+1$. We choose $\sigma_1^{(2)} = 10^{-3}$, so the density varies by 0.1 % between the top and bottom layers. The maximum inertial wavenumber k_{inert} varies linearly with N between $N = 2$ and $N = 11$. This is consistent with our approximate expressions (4.4) and (4.5) for k_{inert}, which indicate that $k_{inert} \sim \varepsilon/\sigma$ for $\varepsilon^2 \ll \sigma$. This gives $k_{inert} \sim \varepsilon N$ when rewritten in terms of N. We expect this linear relationship to continue until $\sigma \approx \varepsilon^2$, i.e. until $N \approx 250$ in this example, at which point the inertial wavenumber should be $k_{inert} \approx 500$. The corresponding dimensional wavelength $\tilde{\lambda}_{inert} \approx 12$ km is then comparable to the total depth of the layer.

Our analysis of the limit $N \to \infty$ is restricted by the difficulty of performing the necessary algebraic manipulations in reasonable time for $N > 11$, even with the aid of symbolic computation. However, our computations for $N \leqslant 11$, and the solutions of (4.3), obtained via the distinguished limit $k = O(\varepsilon)$ as $\varepsilon \to 0$, suggest that as $N \to \infty$ we recover the result for the continuously stratified case found by Gerkema & Shrira (2005*b*), in which there exists a subinertial mode at all wavenumbers. Figure 9(*b*) also highlights the special case of two layers ($N = 2$). The largest inertial wavenumber for $N = 2$ is much smaller than for $N \geqslant 3$ because $k_{inert} \sim \varepsilon/\sqrt{\sigma} \ll \varepsilon/\sigma$, as shown in § 3.4.

https://doi.org/10.1017/jfm.2011.364 Published online by Cambridge University Press

This difference is most easily understood in terms of the rigid-lid limit of the shallow water equations (2.13), as described in the next section.

5. Linear plane waves under the assumption of a rigid lid

In this section we address the behaviour of linear plane waves in the non-traditional shallow water equations under the so-called 'rigid-lid' approximation, in which the uppermost fluid surface is constrained to coincide with a surface of constant gravitational potential. This simplifying assumption is commonly employed in studies of the ocean, ranging from theoretical investigations (e.g. Long 1956) to general circulation models (e.g. Marshall *et al.* 1997). Under the traditional approximation, imposing a rigid lid eliminates the fast surface wave mode, which simplifies the theoretical analysis of internal waves, and also permits a much longer time step in numerical simulations. As we have shown in § 3 and § 4, the wave modes no longer decompose into separate surface and internal modes when non-traditional effects are included. Instead, these modes connect with one another via the long subinertial waves. In this section we show that under the rigid-lid approximation, the internal wave modes connect to one another at long wavelengths in a similar pattern to that described in § 4. The non-traditional shallow water equations under a rigid lid are thus a singular limit of the non-traditional shallow water equations under a free surface, in which the slowest internal modes always connects to the surface mode at sufficiently long wavelengths.

5.1. *Multilayer shallow water equations under an imposed rigid lid*

The rigid-lid multilayer shallow water equations may be derived via the same procedure as outlined in § 2, with the additional constraint that the total thickness of all of the superposed fluid layers must remain constant,

$$\eta_1 = \sum_{i=1}^{N} h_i = \text{constant}. \tag{5.1}$$

We impose a flat upper surface by replacing our earlier assumption of a constant atmospheric pressure at the fluid surface (2.5) with a variable fluid pressure exerted against the rigid lid,

$$p_1 = p_s(x, y, t) \quad \text{at } z = \eta_1. \tag{5.2}$$

This contributes an additional term $(\rho_i/\rho_1)p_s$ to the pressure gradient in the shallow water momentum equation for the ith layer, via the quasihydrostatic pressure given by (2.10). For simplicity of notation, we restrict our attention to the case in which the relative density differences between adjacent layers are all equal, $\sigma_i = (\rho_{i+1} - \rho_i)/\rho_{i+1} = \sigma$. This permits a simplified presentation of the momentum equation by rewriting the density ratios as

$$\frac{\rho_j}{\rho_i} = \prod_{m=j}^{i-1}(1 - \sigma_m) = (1 - \sigma)^{i-j}, \tag{5.3}$$

for any integers $1 \leqslant i < j \leqslant N$. Under this assumption, the rigid-lid equivalent of the

https://doi.org/10.1017/jfm.2011.364 Published online by Cambridge University Press

non-traditional multilayer shallow water momentum equation (2.12) may be written as

$$\frac{\partial \boldsymbol{u}_i}{\partial t} + (\boldsymbol{u}_i \cdot \boldsymbol{\nabla})\boldsymbol{u}_i + \left(\Omega_z - \frac{1}{2}\varepsilon' \boldsymbol{\Omega} \cdot \boldsymbol{\nabla}\,(\eta_i + \eta_{i+1})\right)\hat{\boldsymbol{z}} \times \boldsymbol{u}_i + \frac{1}{2}\varepsilon' \boldsymbol{\Omega} \times \hat{\boldsymbol{z}}\frac{\partial}{\partial t}(\eta_i + \eta_{i+1})$$
$$+ \boldsymbol{\nabla}\left\{(1-\sigma)^{i-1} p_s + \sum_{j=2}^{i} (1-\sigma)^{i-j}\,\eta_j + \frac{1}{2}\varepsilon' h_i (v_i \Omega_x - u_i \Omega_y)\right.$$
$$\left. + \varepsilon' \sum_{j=1}^{i-1} (1-\sigma)^{i-j} h_j \left(v_j \Omega_x - u_j \Omega_y\right)\right\} = 0. \tag{5.4}$$

We have obtained this dimensionless equation by using the internal deformation radius as the horizontal length scale, rather than the external deformation radius used in § 2 to § 4. Our dimensionless variables are thus

$$\boldsymbol{x} = \frac{\tilde{\boldsymbol{x}}}{R_d'}, \quad z = \frac{\tilde{z}}{H}, \quad t = 2\Omega \tilde{t}, \quad \boldsymbol{u}_i = \frac{\tilde{\boldsymbol{u}}_i}{c'}, \quad h_i = \frac{\tilde{h}_i}{H}, \quad p_s = \frac{\tilde{p_s}}{\rho_1 c'^2}, \tag{5.5}$$

where

$$c' = \sqrt{\sigma g H}, \quad R_d' = \frac{c'}{2\Omega}, \quad \varepsilon' = \frac{H}{R_d'} = 2\Omega\sqrt{\frac{H}{\sigma g}}, \tag{5.6}$$

are the internal gravity wave speed, internal deformation radius and internal aspect ratio, respectively.

As in § 4, we linearize about a state of rest, setting $\boldsymbol{u}_i = \boldsymbol{u}_i'$, $h_i = R_i + h_i'$, and neglecting products of primed variables. We seek solutions of the form $\boldsymbol{u}_i', h_i' \sim \exp(\mathrm{i}(k'x - \omega t))$, distinguishing $k' = R_d'\tilde{k}$ from the dimensionless wavenumber $k = R_d\tilde{k}$ used in § 3 and § 4. We obtain a dispersion relation for $\omega(k')$ as a polynomial in ω of order $2N-2$,

$$\omega^{2N-2} + c_{2N-3}\omega^{2N-3} + \cdots + c_1\omega + c_0 = 0. \tag{5.7}$$

This yields $2N-2$ wave modes, two modes fewer than the dispersion relation for the linearized free-surface equations (4.1). Under the traditional approximation this corresponds to removal of the fast surface wave mode, and retention of the slower internal wave modes, both of which are plotted in figure 2 for the case $N = 2$. However, under the complete Coriolis force it is less obvious how the modes plotted in figure 8 should be modified by the rigid-lid constraint.

We investigate the behaviour of the wave modes close to $k' = 0$ following the method described in § 4. The distinguished limit with $k' = O(\varepsilon')$ as $\varepsilon' \to 0$ describes a balance between the gravitational pressure gradient and the non-traditional terms in (5.4). We rescale the wavenumber as $k' = \varepsilon' K'$ with $K' = O(1)$, and pose an asymptotic expansion of the wave frequency $\omega = \omega^{(0)} + \varepsilon'^2\omega^{(1)} + \cdots$. The leading-order term in this expansion is simply the inertial frequency, $\omega^{(0)} = \pm\sin\phi$. The first-order correction $\omega^{(1)}$ describes the universal behaviour in the limit $\varepsilon' \to 0$. In figure 10 we plot $\omega^{(1)}$ against K' using the same parameters as in figure 8, and over the same range of wavenumbers and frequencies. The ranges of the axes differ by a factor of σ between figures 8 and 10, because $K' = k'/\varepsilon' = \sigma k/\varepsilon = \sigma K$. We see a very similar pattern of mode connection through the inertial frequency, with the fastest mode connecting to the slowest mode, the second fastest to the second slowest, and so on. However, all of these connections are between internal modes, as the rigid lid excludes the surface

https://doi.org/10.1017/jfm.2011.364 Published online by Cambridge University Press

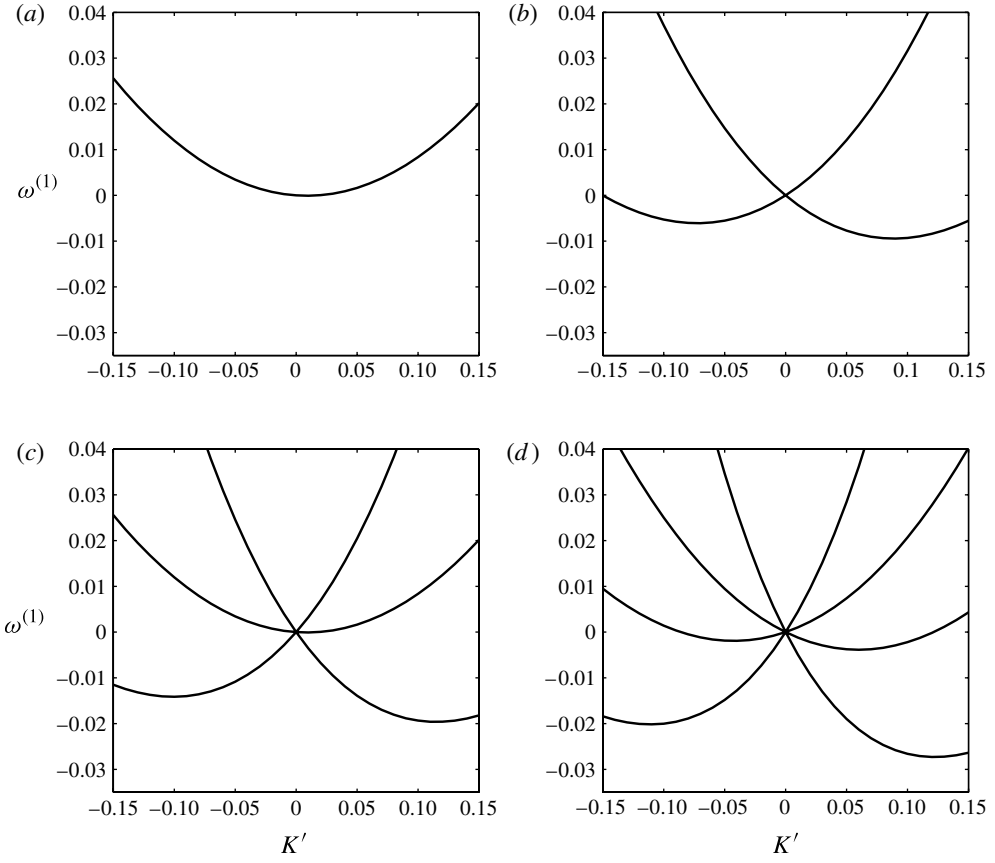


FIGURE 10. Dispersion relations for (*a*) two, (*b*) three, (*c*) four and (*d*) five layers of fluid of equal thickness, governed by the shallow water equations under a rigid lid. The plots have been generated numerically using the distinguished limit $k' = \varepsilon' K'$ with $K' = O(1)$ as $\varepsilon' \to 0$. Thus K' is the scaled dimensionless wavenumber, and $\omega^{(1)}$ is the $O(\varepsilon'^2)$ correction to the inertial frequency $\omega^{(0)} = \sin\phi$. In each case $\phi = \pi/12$, $\theta = \pi/4$ and $\sigma = 0.1$.

mode. The only exception is the case of two layers. This now permits only one wave mode, so no mode connection is possible.

As in § 4, we estimate the range of wavenumbers that are substantially modified by non-traditional effects by calculating the wavenumber at which the frequency matches the inertial frequency. For example, in the case of three layers, solving $\omega^{(1)}(K') = 0$ yields

$$k'_{inert} = \tfrac{1}{2}\varepsilon' \sin(2\phi)(\sigma\cos\theta \pm \sin\theta\sqrt{1-\sigma}). \tag{5.8}$$

These expressions become identical to the two largest values of k_{inert} in (4.4) on setting $\sigma_1 = \sigma_2 = \sigma$, and noting that $k' = \sigma^{1/2}k$ and $\varepsilon' = \sigma^{-1/2}\varepsilon$. For all $N \geqslant 3$ at least two of the inertial wavenumbers satisfy $k'_{inert} \sim \varepsilon'$, or equivalently $k \sim \varepsilon/\sigma$, as we found for the shallow water equations under a free surface in § 4. For $N = 2$ the inertial wavenumber is

$$k'_{inert} = \tfrac{1}{2}\varepsilon'\sigma \sin(2\phi)\cos\theta, \tag{5.9}$$

https://doi.org/10.1017/jfm.2011.364 Published online by Cambridge University Press

which suggests the scaling $k_{inert} \sim \varepsilon$. This differs from the inertial wavenumber (3.21) for the two-layer equations under a free surface, which scales as $k_{inert} \sim \varepsilon/\sqrt{\sigma}$.

5.2. *Asymptotic rigid-lid limit of the multilayer shallow water equations*

To resolve the apparent discrepancy at long wavelengths between the rigid-lid and free-surface multilayer shallow water equations, we consider the asymptotic behaviour of the free-surface equations as they approach the rigid-lid limit. We first rescale the multilayer shallow water equations (2.13)–(2.12), non-dimensionalizing using the internal deformation radius and gravity wave speed, as given by (5.6). The momentum equation for the ith layer is

$$\frac{\partial \boldsymbol{u}_i}{\partial t} + (\boldsymbol{u}_i \cdot \boldsymbol{\nabla})\boldsymbol{u}_i + \left(\Omega_z - \frac{1}{2}\varepsilon' \boldsymbol{\Omega} \cdot \boldsymbol{\nabla}\,(\eta_i + \eta_{i+1})\right)\hat{\boldsymbol{z}} \times \boldsymbol{u}_i + \frac{1}{2}\varepsilon' \boldsymbol{\Omega} \times \hat{\boldsymbol{z}}\frac{\partial}{\partial t}(\eta_i + \eta_{i+1})$$
$$+ \boldsymbol{\nabla}\left\{\frac{1}{\sigma}(1-\sigma)^{i-1}\,\eta_1 + \sum_{j=2}^{i}(1-\sigma)^{i-j}\,\eta_j + \frac{1}{2}\varepsilon' h_i(v_i\Omega_x - u_i\Omega_y)\right.$$
$$\left. + \varepsilon' \sum_{j=1}^{i-1}(1-\sigma)^{i-j}\,h_j\left(v_j\Omega_x - u_j\Omega_y\right)\right\} = 0. \tag{5.10}$$

The rigid-lid equations (5.4) are recovered under an asymptotic expansion of the layer velocities and depths in the relative density difference σ, e.g. $\eta_1 = \eta_1^{(0)} + \sigma\eta_1^{(1)} + \cdots$, holding ε' fixed in the limit $\sigma \to 0$. The ratio of the layer depth to the external deformation radius must then scale as $\varepsilon = H/R_d \sim \sigma^{1/2}$. The leading-order solution is simply $\eta_1^{(0)} = \text{constant}$, and at first order we recover the limit of (5.4) as $\sigma \to 0$, again holding ε' fixed. The first-order correction $\eta_1^{(1)}$ to the upper surface position replaces the surface pressure p_s.

Our investigation of multilayer linear plane waves in § 4 suggests that the limit $\sigma \to 0$ in (5.10) is singular, as the internal wave modes connect to the surface mode close to $k' = 0$. To demonstrate this, we again seek linear plane wave solutions of the form $\boldsymbol{u}_i(x, y, t) = \boldsymbol{u}_i' \exp(\mathrm{i}(k'x - \omega t))$, $h_i(x, y, t) = R_i + h_i' \exp(\mathrm{i}(k'x - \omega t))$, neglecting products of $\boldsymbol{u}_i'$ and h_i'. Under the internal scaling (5.5)–(5.6), the multilayer dispersion relation (4.1) becomes

$$\sigma\omega^{2N} + \sigma(\varepsilon' k' N \cos\phi \cos\theta)\omega^{2N-1} + c_{2N-2}\omega^{2N-2} + \cdots + c_1\omega + c_0 = 0. \tag{5.11}$$

The coefficients $c_0, c_1, \ldots, c_{2N-2}$ differ from their counterparts in (4.1) by factors of σ, and all remain finite in the limit $\sigma \to 0$. Both c_0 and c_{2N-2} contain terms that are $O(\sigma^0)$. The solutions of (5.11) are singular in the limit $\sigma \to 0$ because σ multiplies the highest powers of ω in the dispersion relation. If we pose an asymptotic expansion $\omega = \omega^{(0)} + \sigma\omega^{(1)} + \cdots$, then the leading-order frequency $\omega^{(0)}$ recovers only the $2N - 2$ rigid-lid modes, and higher-order corrections do not capture the surface modes. In the externally scaled dispersion relation (4.1), a similar asymptotic expansion in σ *does* recover all $2N$ modes.

The internal scaling for the multilayer shallow water equations (5.10) highlights two distinguished limits as $k' \to 0$. As in § 3.3, the linearized mass conservation equation (2.12) yields $\eta_i' = O(k')$ as $k' \to 0$. The gravitational pressure gradient $(1/\sigma)\nabla\eta_1$ due to variations of the upper surface balances the non-traditional terms, proportional to ε', when $k' \sim \sigma\varepsilon'$. This is exactly equivalent to the scaling $k \sim \varepsilon$ obtained in § 3, and describes the range of wavenumbers over which the surface mode connects to the slowest internal mode. More formally, in the limit $\sigma \to 0$ we anticipate the

https://doi.org/10.1017/jfm.2011.364 Published online by Cambridge University Press

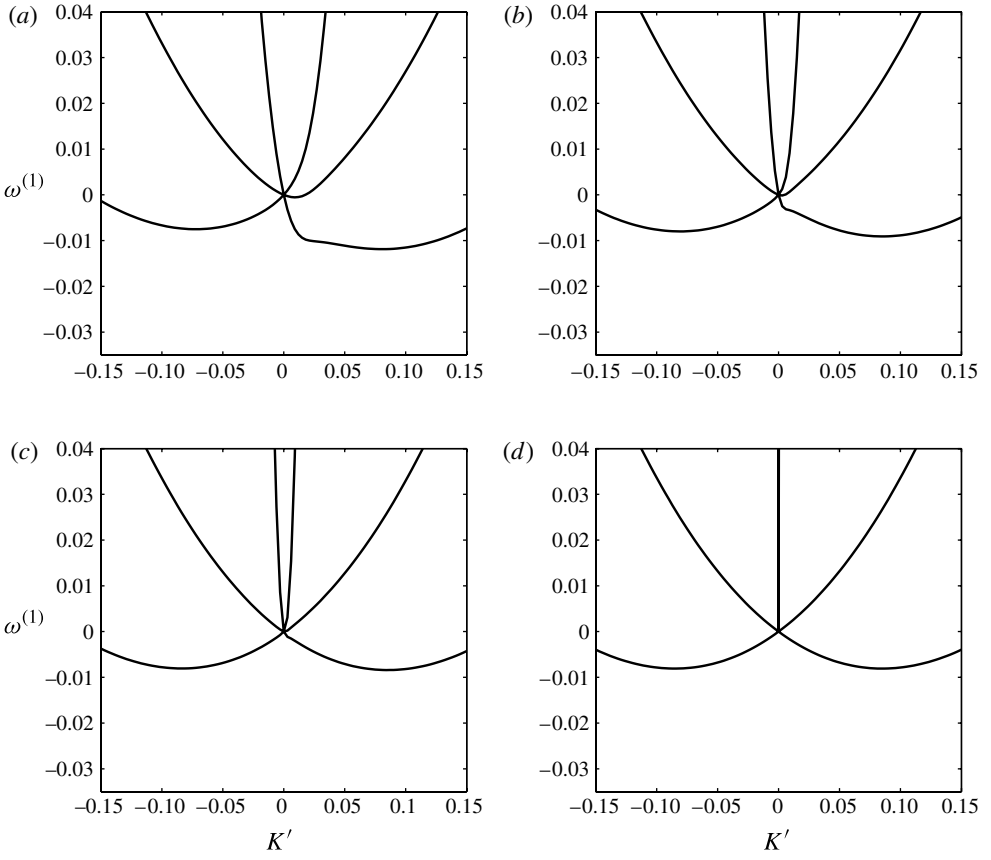


FIGURE 11. Dispersion relation for three layers of equal thickness, scaled by the internal radius of deformation, showing the approach to the limiting case of a rigid lid: (*a*) $\sigma = 10^{-1}$, (*b*) $\sigma = 3 \times 10^{-2}$, (*c*) $\sigma = 10^{-2}$ and (*d*) $\sigma = 10^{-4}$. The plots have been generated numerically using the distinguished limit $k' = \varepsilon' K'$ with $K' = O(1)$ as $\varepsilon' \to 0$. Thus, K' is the scaled dimensionless wavenumber, and $\omega^{(1)}$ is the $O(\varepsilon'^2)$ correction to the inertial frequency $\omega^{(0)} = \sin\phi$. In each case $\phi = \pi/12$ and $\theta = \pi/4$.

distinguished limit $k' = O(\sigma)$, for fixed ε'. Setting $k' = \sigma K'$ and posing an asymptotic expansion $\omega = \omega^{(0)} + \sigma\omega^{(1)} + \cdots$, the leading-order solution is the inertial frequency, $\omega^{(0)} = \pm\sin\phi$. The first-order correction $\omega^{(1)}(K')$ describes the universal behaviour as $k', \sigma \to 0$, capturing the crossing of the surface and internal wave modes through the inertial frequency. Plots of $\omega^{(1)}(K')$ are similar to those shown in figure 8.

The second distinguished limit is $k' = O(\varepsilon')$ as $\varepsilon' \to 0$, for fixed σ, as described in § 5.1. This corresponds to a balance between the gravitational pressure gradients due to variations of the internal surfaces and the non-traditional terms in (5.10). Following the procedure described in § 5.1, we set $k' = \varepsilon' K'$ and pose an asymptotic expansion in ε', $\omega = \omega^{(0)} + \varepsilon'\omega^{(1)} + \cdots$. The leading-order solution is simply the inertial frequency, $\omega^{(0)} = \pm\sin\phi$, and the first-order correction $\omega^{(1)}$ describes the universal behaviour as $k', \varepsilon' \to 0$. In figure 11 we plot $\omega^{(1)}(K')$ for three layers of fluid with the same parameters as used in figure 10. We decrease the stratification σ from 10^{-1} to 10^{-4} to illustrate the approach to the rigid-lid limit as $\sigma \to 0$. The connection of the internal modes to the surface mode is confined to a range of wavenumbers

https://doi.org/10.1017/jfm.2011.364 Published online by Cambridge University Press

where $K' \sim \sigma$. By $\sigma = 10^{-4}$ this region is no longer visible on the internal scaling, and the internal wave modes appear to connect with one another through the inertial frequency, strongly resembling the rigid-lid dispersion relation for three layers in figure 10(*b*). These figures do not match exactly because they correspond to different values of σ, but they approach exact agreement as $\sigma \to 0$.

The approach to the rigid-lid limit also provides an intuitive explanation for the behaviour of the inertial wavenumber k_{inert} in § 4.2. Equations (3.21), (4.4) and (4.5) show that the largest inertial wavenumber satisfies $k_{inert} \sim \varepsilon/\sqrt{\sigma}$ for $N = 2$, but $k_{inert} \sim \varepsilon/\sigma$ for $N \geqslant 3$. This is also illustrated in figure 9(*b*). We obtain the inertial wavenumbers in the distinguished limit $k' = O(\varepsilon')$ by solving $\omega^{(1)}(K') = 0$ for K'. The non-zero inertial wavenumbers in two, three and four layers are, respectively,

$$K'_{inert,2} = \tfrac{1}{2}\sin(2\phi)\left(\sigma\cos\theta \pm \sin\theta\sqrt{\sigma(1-\sigma)}\right), \tag{5.12}$$

$$K'_{inert,3} = \tfrac{1}{2}\sigma\sin(2\phi)\cos\theta,\ \ \tfrac{1}{2}\sin(2\phi)\left(\sigma\cos\theta \pm \sin\theta\sqrt{1-\sigma^2}\right), \tag{5.13}$$

$$K'_{inert,4} = \tfrac{1}{2}\sin(2\phi)\left\{\sigma\cos\theta \pm_\alpha \sin\theta\sqrt{(1-\sigma)\left(1+\tfrac{1}{2}\sigma \pm_\beta \sqrt{1+\tfrac{1}{4}\sigma^2}\right)}\right\}. \tag{5.14}$$

In two layers the inertial wavenumber satisfies $K'_{inert,2} \sim \sigma^{1/2}$ as $\sigma \to 0$, and the largest inertial wavenumbers in the three- and four-layer cases satisfy $K'_{inert,N} \sim 1$ as $\sigma \to 0$. However, one of the inertial wavenumbers in the three-layer case satisfies $K'_{inert,3} \sim \sigma$ as $\sigma \to 0$, and two of the inertial wavenumbers in the four-layer case satisfy $K'_{inert,4} \sim \sigma^{1/2}$ as $\sigma \to 0$. We conjecture that this pattern extends to the general case of N layers. For N odd, one of the inertial wavenumbers satisfies $K'_{inert,N} \sim \sigma$ as $\sigma \to 0$. This wavenumber corresponds to the unconnected wave mode and vanishes in the limit $\sigma \to 0$ (see figure 11). The remaining $N-1$ inertial wavenumbers satisfy $K'_{inert,N} \sim 1$ as $\sigma \to 0$. For N even, two of the inertial wavenumbers satisfy $K'_{inert,N} \sim \sigma^{1/2}$ as $\sigma \to 0$. The corresponding wave modes connect to one another as $\sigma \to 0$, leading to a single unconnected mode in the rigid-lid limit (see figure 10(*a*,*c*)). The remaining $N-2$ inertial wavenumbers satisfy $K'_{inert,N} \sim 1$ as $\sigma \to 0$. We have verified this conjecture up to $N = 10$ via direct computation of the dispersion relation in the distinguished limit $k' = O(\varepsilon')$. Thus, in order for any inertial wavenumber to satisfy $K'_{inert,N} \sim 1$ as $\sigma \to 0$, the number of layers N must be large enough to support inter-connection of internal modes in the rigid-lid limit. It is therefore not surprising that the largest inertial wavenumber scales differently in one or two layers, as illustrated in figure 9(*b*), than it does in three or more layers.

6. Conclusion

The traditional multilayer shallow water equations have been used widely as a conceptual model for many oceanographic phenomena. By capturing interactions between barotropic and baroclinic modes, they offer a better model for the behaviour of a continuously stratified fluid than the single-layer shallow water equations (e.g. LeBlond & Mysak 1978). Following the single-layer work of Dellar & Salmon (2005), Stewart & Dellar (2010) extended the multilayer shallow water equations to include the complete Coriolis force, while retaining all of the expected conservation properties for energy, momentum and potential vorticity. In this paper we have demonstrated that the additional 'non-traditional' terms in the equations dramatically change the properties of long linear plane waves.

https://doi.org/10.1017/jfm.2011.364 Published online by Cambridge University Press

Our study of the dispersion relation for linear plane waves in the two-layer equations and of the eigenvectors relating the perturbations h_1', h_2', etc., indicates a number of differences from the behaviour under the traditional approximation. Again, the horizontal component of the rotation vector defines a preferred direction, so the dispersion relation becomes horizontally anisotropic. This anisotropy is manifested in the east/west asymmetry of the dispersion relation plotted in figure 2.

The two-layer equations support two wave modes, which may typically be identified either as surface (barotropic) waves, in which the height perturbations h_1' and h_2' oscillate in phase, or as internal (baroclinic) waves in which the height perturbations oscillate π radians out of phase. Under the traditional approximation, this separation into surface and internal waves persists at all wavelengths, and the dimensional frequencies $\tilde{\omega}$ of the wave modes are bounded below by the inertial frequency $2\Omega|\sin\phi|$. Including the complete Coriolis force permits a range of long waves with frequencies below the inertial frequency. These were named 'subinertial' waves by Gerkema & Shrira (2005*a*,*b*). Subinertial waves exhibit $O(1)$ modifications in their structure due to the non-traditional components of the Coriolis force, as shown in figure 6, so they no longer qualify as either surface or internal waves. Moreover, eastward propagating surface waves connect with westward-propagating internal waves via the long subinertial waves and vice versa. This is an example of a mode conversion, also known as a Landau–Zener transition, between two types of wave (e.g. Craik 1985; Flynn & Littlejohn 1994). Other examples of mode conversion in oceanic flows include topographic coupling between Rossby waves in a multi-layer system (Vanneste 2001; Tailleux & McWilliams 2002) and coupling between internal gravity waves and vortical waves in stratified shear flows (Voronovich, Shrira & Stepanyants 1998). Mode conversions are particularly common in Hamiltonian systems, due to the tendency of their eigenvalues to avoid crossing (Landau & Lifshitz 1977, § 99).

The long subinertial waves in our two-layer equations share many qualitative properties with the subinertial waves in continuously stratified fluids identified by Gerkema & Shrira (2005*a*,*b*). For example, both types of waves connect branches of waves that are unconnected under the traditional approximation. Both types of subinertial waves also exhibit universal behaviours at near-inertial frequencies, and their existence reflects the singular nature of the traditional approximation as a perturbation in ε. In this respect, the existence of long waves is more surprising than the existence of short waves. Short waves introduce a short horizontal length scale that is closer in magnitude to the vertical length scale. One might thus expect the traditional approximation, being based on a small aspect ratio, to become invalid for sufficiently short waves. Conversely, one would expect the traditional approximation to hold especially well for long waves.

Our analysis in § 3.3 shows that this counterintuitive effect on long waves may be explained in terms of a distinguished asymptotic limit. This limit is characterized by waves whose dimensionless wavelength, relative to the Rossby deformation radius R_d, is comparable to the aspect ratio $\varepsilon = H/R_d$. Comparing the magnitudes of terms in the horizontal momentum equations, this distinguished limit arises because the pressure gradient is $O(k^2)$ for disturbances with dimensionless wavenumber k, while the non-traditional terms are $O(\varepsilon k)$. For sufficiently long waves the formally small non-traditional effects thus appear at leading order in the momentum equation. There is an $O(1)$ change in the structure of these waves for arbitrarily small ε, the conventional measure of the strength of non-traditional effects, so the linear wave solution under the traditional approximation is singularly perturbed. Our scaling corresponds to the

https://doi.org/10.1017/jfm.2011.364 Published online by Cambridge University Press

scaling used by Thuburn *et al.* (2002*b*) for shallow near-inertial waves if we identify $\varepsilon = H/R_d$ with the natural aspect ratio $\kappa = 2\Omega/N$ for a continuously stratified fluid.

In the shallow water equations with three or more layers, the fast barotropic wave mode always connects to the slowest baroclinic mode through the subinertial wavenumbers. This mode always attains the lowest subinertial frequency, and encompasses the largest range of subinertial wavenumbers. For a fluid with fixed total equilibrium depth and fixed total density variation, the maximum inertial wavenumber k_{inert} varies linearly with N as long as the relative density difference σ between layers satisfies $\sigma \gg \varepsilon^2$. It is plausible that $k_{inert} \to \infty$ as $N \to \infty$, which would be consistent with the results of Gerkema & Shrira (2005*b*) for waves in a continuously stratified fluid. However, demonstrating this is difficult due to the complicated algebra associated with the linear wave problem for many discrete layers.

The barotropic mode vanishes if a rigid lid is imposed at the upper surface, and instead the internal modes connect to one another via the inertial frequency. These interconnections follow a similar pattern, with the fastest baroclinic mode connecting to the slowest baroclinic mode via subinertial wavenumbers. The rigid-lid shallow water equations are thus a singular limit of the free-surface shallow water equations, as different wave modes connect to one another through the inertial frequency. When non-dimensionalized by the internal radius of deformation, as in (5.6), the free-surface modes approach the rigid-lid modes in the limit $\sigma \to 0$ with $\sigma^{1/2}k$ and $\sigma^{-1/2}\varepsilon$ held fixed. The barotropic mode still exists and connects to the internal modes at very long wavelengths, where $k = O(\varepsilon)$, but these wavelengths are much too large ($\gtrsim 10^6$ km) to exist on Earth.

The inertial wavenumber k_{inert} provides a useful estimate of the wavelength at which linear plane waves are strongly affected by the inclusion of the complete Coriolis force. In § 4.2 we show that for $N > 2$, the largest inertial wavenumber is proportional to ε and inversely proportional to σ for all but east/west-propagating waves,

$$k_{inert} \sim \frac{\varepsilon}{\sigma} \quad \text{or} \quad \tilde{\lambda}_{inert} \sim \frac{\sigma g}{\Omega^2}, \tag{6.1}$$

where $\tilde{\lambda}_{inert}$ is the dimensional inertial wavelength. For Earth-like parameters and weak stratification ($\sigma = 10^{-4}$), this inertial wavelength is about 180 km, which is typical for large-scale ocean waves. Above this wavelength, oscillations of the internal surfaces associated with the slowest baroclinic mode must be accompanied by substantial oscillations of the free surface, as illustrated in figure 6. As oscillations of the free surface require much more energy than oscillations of an internal surface for a given amplitude, internal wave propagation may be constrained by the non-traditional components of the Coriolis force. The longest waves, which carry the most energy, are most strongly affected by this change in structure, which makes this a relevant consideration for internal waves in the real ocean.

Although the multilayer dispersion relation appears to approach the continuously stratified dispersion relation of Gerkema & Shrira (2005*b*) as the number of layer tends to infinity (see § 4), it remains to be seen whether waves in continuously stratified fluid exhibit similar structural changes and patterns of mode reconnection. The multilayer shallow water equations are a highly idealized model of a continuously stratified fluid, restricting density variations to a series of discontinuous jumps between homogeneous layers. They are most accurately applied to near-homogeneous layers of fluid separated by rapid changes in density, so we may expect our results to apply to similar regions in the ocean. Moreover, the scaling arguments used in § 3.3 identify a distinguished limit in which non-traditional effects become comparable to

https://doi.org/10.1017/jfm.2011.364 Published online by Cambridge University Press

the horizontal gradient of the hydrostatic pressure. This scaling appears to apply equally well to a continuously stratified fluid.

In this paper we have only considered linear plane waves on a non-traditional f-plane, but the non-traditional components of the Coriolis force may be important in a broad range of oceanic and atmospheric waves (e.g. Thuburn *et al.* 2002*a*,*b*; Kasahara 2003, 2007; Kasahara & Gary 2010; Gerkema & Shrira 2005*a*,*b*). For example, we might expect non-traditional effects to be most pronounced close to the equator, where the rotation vector lies almost parallel to the planet's surface, and our f-plane approximation breaks down. Near-equatorial waves must therefore be treated as a separate case, as in the single-layer study of Dellar & Salmon (2005). The shallow water equations also serve as a useful idealized model for nonlinear ocean waves. The non-traditional terms in (3.1*a*) are all nonlinear, so we might expect nonlinear waves to show interesting deviations due to non-traditional effects. We have also completely neglected the influence of bottom topography. The vertical velocity of fluid moving up or down a slope is coupled with the east/west velocity by non-traditional effects. The presence of varying bottom topography at $z = h_b(x, y)$ thus changes the effective Coriolis parameter that appears in the single-layer shallow water potential vorticity from f to $f_{eff} = f - \boldsymbol{\nabla} \cdot ((h_b + \frac{1}{2}h)\boldsymbol{\Omega})$, and similarly for multiple layers. Here $\boldsymbol{\Omega}$ is the dimensional horizontal component of the rotation vector and $f = 2\Omega \sin\phi$ is the traditional Coriolis parameter. Topographic variations may thus substantially influence the large-scale flow through non-traditional effects. For instance, Stewart & Dellar (2011*a*,*b*) found that this mechanism substantially influences the transport of fluid across the equator by abyssal ocean currents flowing through channel-like topography. Looking to wider applications, we expect non-traditional effects to be even more pronounced on Jupiter, which has a larger rotation rate, and a much larger radius, although stronger gravity. Using the estimate (6.1) with parameters from Dowling & Ingersoll (1989) suggests that non-traditional effects should become pronounced at $\tilde{\lambda}_{inert} \approx 80\,\text{km}$, so virtually all wavelengths large enough to contribute to planetary-scale atmospheric motions on Jupiter should be strongly affected by the non-traditional part of the Coriolis force.

A.L.S. is supported by an EPSRC PhD Plus award, and previously by a EPSRC Doctoral Training Account award. The research of P.J.D. is supported by an EPSRC Advanced Research Fellowship, grant number EP/E054625/1.

REFERENCES

ABRAMOWITZ, M. & STEGUN, I. A. 1965 *Handbook of Mathematical Functions*. Dover.

BLECK, R. & CHASSIGNET, E. 1994 Simulating the oceanic circulation with isopycnic-coordinate models. In *The Oceans: Physical–Chemical Dynamics and Human Impact* (ed. S. Majumdar, E. Miller, G. Forbe, R. Schmalz & A. Panah), pp. 17–39. Pennsylvania Acad. Sci.

BLECK, R., ROOTH, C., HU, D. & SMITH, L. T. 1992 Salinity-driven thermocline transients in a wind- and thermohaline-forced isopycnic coordinate model of the North Atlantic. *J. Phys. Oceanogr.* **22**, 1486–1505.

BOSS, E., PALDOR, N. & THOMPSON, L. 1996 Stability of a potential vorticity front: from quasi-geostrophy to shallow water. *J. Fluid Mech.* **315**, 65–84.

BOTTE, V. & KAY, A. 2002 A model of the wind-driven circulation in Lake Baikal. *Dyn. Atmos. Oceans* **35**, 131–152.

CRAIK, A. D. D. 1985 *Wave Interactions and Fluid Flows*. Cambridge University Press.

CULLEN, M. J. P. 1993 The unified forecast/climate model. *Meteorol. Mag.* **122**, 81–94.

https://doi.org/10.1017/jfm.2011.364 Published online by Cambridge University Press

DELLAR, P. J. 2011 Variations on a beta-plane: derivation of non-traditional beta-plane equations from Hamilton's principle on a sphere. *J. Fluid Mech.* **674**, 174–195.

DELLAR, P. J. & SALMON, R. 2005 Shallow water equations with a complete Coriolis force and topography. *Phys. Fluids* **17**, 106601–19.

DOWLING, T. E. & INGERSOLL, A. P. 1989 Jupiter's Great Red Spot as a shallow water system. *J. Atmos. Sci.* **46**, 3256–3278.

ECKART, C. 1960 *Hydrodynamics of Oceans and Atmospheres*. Pergamon.

FLYNN, W. G. & LITTLEJOHN, R. G. 1994 Normal forms for linear mode conversion and Landau–Zener transitions in one dimension. *Ann. Phys.* **234**, 334–403.

FU, L. -L. 1981 Observations and models of inertial waves in the deep ocean. *Rev. Geophys.* **19**, 141–170.

GERKEMA, T. & EXARCHOU, E. 2008 Internal-wave properties in weakly stratified layers. *J. Mar. Res.* **66**, 617–644.

GERKEMA, T. & SHRIRA, V. I. 2005*a* Near-inertial waves in the ocean: beyond the 'traditional approximation'. *J. Fluid Mech.* **529**, 195–219.

GERKEMA, T. & SHRIRA, V. I. 2005*b* Near-inertial waves on the non-traditional β-plane. *J. Geophys. Res.* **110**, C10003.

GERKEMA, T., ZIMMERMAN, J. T. F., MAAS, L. R. M. & VAN HAREN, H. 2008 Geophysical and astrophysical fluid dynamics beyond the traditional approximation. *Rev. Geophys.* **46**, RG2004.

GILL, A. E. 1982 *Atmosphere Ocean Dynamics*. Academic Press.

VAN HAREN, H. & MILLOT, C. 2004 Rectilinear and circular inertial motions in the Western Mediterranean Sea. *Deep-Sea Res.* **51**, 1441–1455.

VAN HAREN, H. & MILLOT, C. 2005 Gyroscopic waves in the Mediterranean Sea. *Geophys. Res. Lett.* **32**, L24614.

HENDERSHOTT, M. C. 1981 Long waves and ocean tides. In *Evolution of Physical Oceanography* (ed. B. A. Warren & C. Wunsch), pp. 292–341. Massachusetts Institute of Technology Press.

HUGHES, B. 1964 Effect of rotation on internal gravity waves. *Nature* **201**, 798–801.

KASAHARA, A. 2003 The roles of the horizontal component of the Earth's angular velocity in nonhydrostatic linear models. *J. Atmos. Sci.* **60**, 1085–1095.

KASAHARA, A. 2007 Initial-value approach to study the inertio-gravity waves without the 'traditional approximation'. *J. Comput. Phys.* **225**, 2175–2197.

KASAHARA, A. & GARY, J. M. 2010 Studies of inertio-gravity waves on midlatitude beta-plane without the traditional approximation. *Q. J. R. Meteorol. Soc.* **136**, 517–536.

LANDAU, L. D. & LIFSHITZ, E. 1977 *Quantum Mechanics: Non-Relativistic Theory*, 3rd edn. Butterworth–Heinemann.

LEBLOND, P. H. & MYSAK, L. A. 1978 *Waves in the Ocean*. Elsevier.

LEIBOVICH, S. & LELE, S. K. 1985 The influence of the horizontal component of Earth's angular velocity on the instability of the Ekman layer. *J. Fluid Mech.* **150**, 41–87.

LONG, R. R. 1956 Long waves in a two-fluid system. *J. Met.* **13**, 70–74.

MARSHALL, J., HILL, C., PERELMAN, L. & ADCROFT, A. 1997 Hydrostatic, quasi-hydrostatic, and nonhydrostatic ocean modelling. *J. Geophys. Res.* **102**, 5733–5752.

MARSHALL, J. & SCHOTT, F. 1999 Open-ocean convection: observations, theory, and models. *Rev. Geophys.* **37**, 1–64.

MUNK, W. 1981 Internal waves and small-scale processes. In *Evolution of Physical Oceanography* (ed. B. A. Warren & C. Wunsch), pp. 264–291. Massachusetts Institute of Technology Press.

MUNK, W. & PHILLIPS, N. 1968 Coherence and band structure of inertial motion in the sea. *Rev. Geophys.* **6**, 447–472.

NOF, D. & OLSON, D. B. 1993 How do western abyssal currents cross the equator? *Deep-Sea Res.* **40**, 235–255.

PEDLOSKY, J. 1987 *Geophysical Fluid Dynamics*, 2nd edn. Springer.

PHILLIPS, N. A. 1954 Energy transformations and meridional circulations associated with simple baroclinic waves in a two-level, quasi-geostrophic model. *Tellus* **6**, 273–286.

https://doi.org/10.1017/jfm.2011.364 Published online by Cambridge University Press

PHILLIPS, N. A. 1968 Reply to Comment by Veronis. *J. Atmos. Sci.* **25**, 1155–1157.

PHILLIPS, N. A. 1973 Principles of large scale numerical weather prediction. In *Dynamic Meteorology: Lectures Delivered at the Summer School of Space Physics of the Centre National d'Études Spatiales* (ed. P. Morel), pp. 3–96. D. Reidel Pub. Co.

SAINT-GUILY, B. 1970 On internal waves. Effects of the horizontal component of the Earth's rotation and of a uniform current. *Dtsch. Hydrogr. Z.* **23**, 16–23.

SALMON, R. 1982 The shape of the main thermocline. *J. Phys. Oceanogr.* **12**, 1458–1479.

SALMON, R. 1998 *Lectures on Geophysical Fluid Dynamics*. Oxford University Press.

STEWART, A. L. & DELLAR, P. J. 2010 Multilayer shallow water equations with complete Coriolis force. Part I. Derivation on a non-traditional beta-plane. *J. Fluid Mech.* **651**, 387–413.

STEWART, A. L. & DELLAR, P. J. 2011*a* The rôle of the complete Coriolis force in cross-equatorial flow of abyssal ocean currents. *Ocean Model.* **38**, 187–202.

STEWART, A. L. & DELLAR, P. J. 2011*b* Cross-equatorial flow through an abyssal channel under the complete Coriolis force: two-dimensional solutions. *Ocean Model.* **40**, 87–104.

TAILLEUX, R. & MCWILLIAMS, J. C. 2002 Energy propagation of long extratropical Rossby waves over slowly varying zonal topography. *J. Fluid Mech.* **473**, 295–319.

THUBURN, J., WOOD, N. & STANIFORTH, A. 2002*a* Normal modes of deep atmospheres. I: spherical geometry. *Q. J. R. Meteorol. Soc.* **128**, 1771–1792.

THUBURN, J., WOOD, N. & STANIFORTH, A. 2002*b* Normal modes of deep atmospheres. II: f-F-plane geometry. *Q. J. R. Meteorol. Soc.* **128**, 1793–1806.

VALLIS, G. K. 2006 *Atmospheric and Oceanic Fluid Dynamics*. Cambridge University Press.

VANNESTE, J. 2001 Mode conversion for Rossby waves over topography: comments on 'Localized coupling between surface- and bottom-intensified flow over topography'. *J. Phys. Oceanogr.* **31**, 1922–1925.

VORONOVICH, V. V., SHRIRA, V. I. & STEPANYANTS, Y. A. 1998 Two-dimensional models for nonlinear vorticity waves in shear flows. *Stud. Appl. Maths* **100**, 1–32.

WHITE, A. A. 2002 A view of the equations of meteorological dynamics and various approximations. In *Large-scale Atmosphere–Ocean Dynamics 1: Analytical Methods and Numerical Models* (ed. J. Norbury & I. Roulstone), pp. 1–100. Cambridge University Press.

WHITE, A. A. & BROMLEY, R. A. 1995 Dynamically consistent, quasi-hydrostatic equations for global models with a complete representation of the Coriolis force. *Q. J. R. Meteorol. Soc.* **121**, 399–418.

WHITE, A. A., HOSKINS, B. J., ROULSTONE, I. & STANIFORTH, A. 2005 Consistent approximate models of the global atmosphere: shallow, deep, hydrostatic, quasi-hydrostatic and non-hydrostatic. *Q. J. R. Meteorol. Soc.* **131**, 2081–2107.

WHITHAM, G. B. 1974 *Linear and Nonlinear Waves*. Wiley Interscience.

WU, T. Y. 1981 Long waves in ocean and coastal waters. *J. Engng Mech. ASCE* **107**, 501–522.

ZEITLIN, V. 2007 *Nonlinear Dynamics of Rotating Shallow Water: Methods and Advances*. Elsevier.

https://doi.org/10.1017/jfm.2011.364 Published online by Cambridge University Press